Search for the lepton flavor violating decay $A^0/H^0 \to \tau^{\pm}\mu^{\mp}$ at hadron colliders

Kétévi A. Assamagan*
Department of Physics, Brookhaven National Laboratory, Upton, New York 11973

Aldo Deandrea† and Pierre-Antoine Delsart‡
Institut de Physique Nucléaire, Université Lyon I, 4 rue E. Fermi, F-69622 Villeurbanne Cedex, France
(Received 12 August 2002; published 7 February 2003)

In the two Higgs doublet model type III and in several other extensions of the standard model, there are no discrete symmetries that suppress flavor changing couplings at the tree level. The experimental observation of the $\nu_\mu - \nu_\tau$ flavor oscillation may suggest the non-conservation of the lepton number. This would lead to the decay of the type $A^0/H^0 \to \tau^{\pm}\mu^{\mp}$. We determine the present low energy limit on lepton flavor violating (LFV) couplings from the muon $g-2$ measurement and discuss the prospects for detecting lepton flavor violating decays at the Fermilab Tevatron and at the CERN Large Hadron Collider. The achievable bounds on the LFV coupling parameter $\lambda_{\tau\mu}$ are presented.

DOI: 10.1103/PhysRevD.67.035001 PACS number(s): 12.60.Fr, 11.30.Hv, 14.80.Cp

I. MOTIVATION

In the standard model (SM), lepton flavor is conserved separately for each generation. The diagonalization of the up-type and down-type mass matrices ensures the diagonalization of the Higgs-fermion coupling matrices [1]: the interaction term of the neutral fields in the SM can be written as

$$\mathcal{L}_Y = -h_{ij}\bar{\psi}_i\psi_j\phi. \tag{1}$$

The spontaneous electroweak symmetry breaking gives the mass matrix

$$M_{ij} = h_{ij}\langle\phi\rangle. \tag{2}$$

Diagonalizing M_{ij} also diagonalizes the Yukawa coupling matrix h_{ij}. The severe experimental limits on the existence of flavor changing neutral currents place stringent constraints on the flavor changing sector of extended models [2] where lepton flavor violation (LFV) may appear at the tree level or may be induced at higher orders. In the minimal supersymmetric standard model (MSSM) the flavor problem is related to the soft supersymmetry breaking mass terms. In the basis where the lepton mass matrix is diagonalized, if there are non-zero off-diagonal matrix elements in the slepton mass matrix, LFV is introduced via loop contributions involving slepton mixing. There are many ways to avoid LFV, for example gravity [3] or gauge-mediated [4] supersymmetry breaking, or flavor symmetries [5]. In the minimal supergravity (SUGRA) model the supersymmetry breaking mass terms have a universal structure at a high scale of the order of the Planck scale. However, LFV effects can be induced by radiative corrections [6]. Large LFV effects can arise in supersymmetric models (SUSY) with a right-handed Majorana neutrino [7–10] and in SUSY with *R*-parity violation [11].

In general, in models with several Higgs doublets, the up-type quarks and the down-type quarks can simultaneously couple to more than a single scalar doublet. As a result, the same operators do not diagonalize the mass matrices and the Higgs-fermion couplings, leading to the prediction of flavor changing neutral current (FCNC) at the tree level. For instance, in the two Higgs doublet model (2HDM), the Yukawa interaction Lagrangian (for the neutral fields) can be written as

$$\mathcal{L}_Y = -f_{ij}\bar{\psi}_i\psi_j\varphi_1 - g_{ij}\bar{\psi}_i\psi_j\varphi_2 \tag{3}$$

which gives, after spontaneous electroweak symmetry breaking, a mass matrix of the form

$$M_{ij} = f_{ij}\langle\varphi_1\rangle + g_{ij}\langle\varphi_2\rangle. \tag{4}$$

When this matrix M_{ij} is diagonalized, the coupling matrices f_{ij} and g_{ij} are not, in general, diagonalized. To suppress the tree level FCNC in the theory so as not to be in conflict with known experimental limits, an *ad hoc* discrete symmetry is invoked [12] whereby the fermions of a given electric charge could couple to no more than one Higgs doublet. In the 2HDM, the up-type and the down-type quarks couple either to the same Higgs doublet (this is known as the 2HDM-I), or they could couple to different doublets (2HDM-II). One of the most stringent tests of the 2HDM type I and type II comes from the measurement of the $b \to s\gamma$ decay rate which receives substantial enhancement (over the SM prediction) in the 2HDM in a large region of the $(m_{H^{\pm}}, \tan\beta)$ parameter space [13–15]. The measured $b \to s\gamma$ decay rate from CLEO [16] and ALEPH [17] leads to a model-dependent indirect lower bound of the charged Higgs mass as function of $\tan\beta$ [18].

In the 2HDM-III, no discrete symmetries are present and in general FCNC exist in this model [19,20]. As an example the LFV interaction Lagrangian of the light neutral Higgs boson h of the 2HDM-III type b (see the Appendix for details) is

*Electronic address: ketevi@bnl.gov
†Electronic address: deandrea@ipnl.in2p3.fr
‡Electronic address: delsart@ipnl.in2p3.fr

$$-\mathcal{L}_{LFV}=h_{ij}\ \overline{l}_i l_j h+\text{H.c.}=\xi_{ij}\frac{\cos(\alpha-\beta)}{\sqrt{2}\cos\beta}\ \overline{l}_i l_j h+\text{H.c.} \tag{5}$$

where α is the mixing angle of the neutral Higgs sector, ξ_{ij} the Yukawa LFV couplings and i, j are the generation indices (in the following the notation h_{ij} will be used to indicate the generic Yukawa coupling, including the mixing angles). To be consistent with experimental data on K^0-$\overline{K^0}$, D^0-$\overline{D^0}$ and B^0-$\overline{B^0}$ mixing, which put stringent constraints on flavor changing couplings with the first generation index, and since one might expect the biggest contribution to come from the LFV couplings of the second and the third generation (ξ_{sb}, $\xi_{\tau\mu}$, ξ_{ct}), these couplings have been parametrized as a function of the masses of the fermions involved since a natural hierarchy is found in the fermion masses [2]:

$$\xi_{ij}=\lambda_{ij}\frac{\sqrt{m_i m_j}}{v}, \tag{6}$$

where $v\simeq 246$ GeV and the residual arbitrariness of flavor changing couplings is expressed by the parameters λ_{ij} which is constrained by experimental bounds on FCNC and LFV processes. A similar hierarchy will be assumed for the LFV coupling η_{ij} of 2HDM-III type a—see the Appendix. In the charged Higgs boson decays this implies a zero LFV coupling if the neutrino is massless and in general a suppression proportional to the square root of the small neutrino mass. We also consider an alternative case in which we drop the neutrino mass dependence for the charged Higgs LFV couplings and adopt instead the same parametrization as in the neutral Higgs sector. In the numerical analysis of the muon anomalous magnetic moment, this distinction is not important as the charged Higgs contribution is small in both cases and can be neglected in comparison to the neutral ones for the range of masses and mixing angles considered.

II. LOW ENERGY BOUNDS

In the purely leptonic sector, the $\mu\to e\gamma$ conversion process gives $\sqrt{\lambda_{\tau\mu}\lambda_{e\tau}}<5$ [21]. It would be desirable to examine a process that depends only on a single coupling. The K^0-$\overline{K^0}$, D^0-$\overline{D^0}$ and B^0-$\overline{B^0}$ mixing depend on a single coupling and data on these processes give $\lambda_{ds}<0.2$, $\lambda_{db}<0.25$ and $\lambda_{uc}<0.6$, assuming 500 GeV for the mass of the pseudoscalar which gives the strongest bound [19]. One sees that LFV coupling with the first generation indices is severely constrained. Another process with a single LFV coupling is the muon anomalous magnetic moment $a_\mu=(g_\mu-2)/2$ [22] where high precision data [23] can be used to constrain $\lambda_{\tau\mu}$, by comparing the measured a_μ to the theoretical prediction of the SM. The new experimental world average reads [23]:

$$a_\mu^{\text{exp}}=11659203(8)\times 10^{-10}. \tag{7}$$

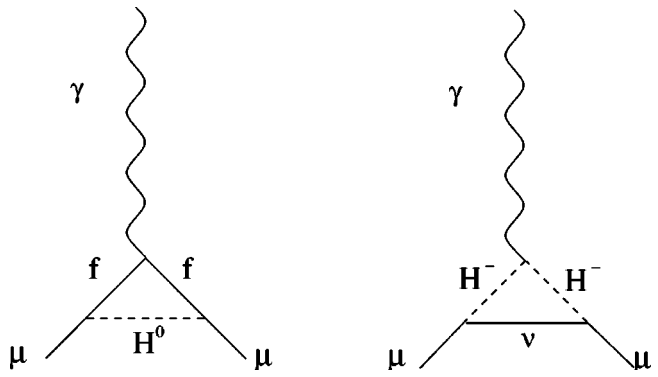

FIG. 1. The one-loop contributions of the Higgs sector to a_μ. H^0 stands for a generic neutral Higgs boson, f is a lepton. With $f=\mu$ we obtain the flavor conserving contribution, with $f=\tau$ the LFV one. As explained in the text we neglect the LFV contribution with $f=e$.

Recently, the standard model calculation was revised in order to take into account the correct sign for the light by light hadronic contribution [24] and the standard model expectation is

$$a_\mu^{\text{SM}}=11659177(7)\times 10^{-10}. \tag{8}$$

Another often quoted value is

$$a_\mu^{\text{SM}}=11659186(8)\times 10^{-10} \tag{9}$$

which gives only slightly more restrictive figures if used to bound the LFV couplings. In the following we shall use the value of Eq. (8). Note that a recent evaluation of the light by light hadronic correction [25] based on chiral perturbation theory suggests that the theoretical error due to unknown low energy constants from sub-leading contributions may increase the estimated error. The difference between experiment and the SM theoretical calculation is

$$\Delta a_\mu=a_\mu^{\text{exp}}-a_\mu^{\text{SM}}=26(11)\times 10^{-10}. \tag{10}$$

We obtain the 90% confidence level (C.L.) range on Δa_μ

$$8\times 10^{-10}\leqslant\Delta a_\mu\leqslant 44\times 10^{-10} \tag{11}$$

to constrain new physics. In the following we shall consider the effect of flavor violating Higgs-leptons interactions plus the flavor conserving Higgs bosons contributions as the only additional ones with respect to the SM. At the one-loop level the Feynman diagrams are those of Fig. 1 and the contribution to a_μ is given for a large class of models by [26] (see also the erratum in [1] concerning other results in the literature), and can be used to obtain the one-loop Higgs contributions to a_μ for the model considered in this paper:

$$\Delta a_\mu^N=\frac{h_{\mu f}^2 m_\mu^2}{8\pi^2}\int_0^1\frac{x^2(1-x)\pm x^2(m_f/m_\mu)}{m_\mu^2 x^2+x(m_f^2-m_\mu^2)+(1-x)m_H^2}dx \tag{12}$$

for a neutral Higgs boson and the sign is $+$ $(-)$ for the scalar (pseudo-scalar). h_{ij} is here a generic Yukawa coupling,

TABLE I. The four sets of parameters used to obtain bounds on the LFV couplings. Sets 1–3 are consistent with the relations between the masses and mixing angles obtained at one loop within the MSSM [27] in order to allow for a comparison. Note, however, that the 2HDM-III is not constrained by the symmetries imposed on MSSM in order to avoid the tree-level LFV. Set 4 corresponds to a choice of parameters that is not allowed in MSSM. Masses are in GeV and the angle α in rad.

Set	m_h	m_H	m_A	$m_{H^\pm}$	α	$\tan\beta$
(1)	93	134	100	127	0.4	5
(2)	127	131	129	160	-0.58	45
(3)	128	500	496	509	0	50
(4)	125	200	200	250	0.2	10

whose expression in terms of η_{ij} or ξ_{ij} and the angles α, β can be read in the Lagrangian given in the Appendix. m_f is the mass of the muon for the flavor conserving contribution with coupling $h_{\mu\mu}$, and $m_f=m_\tau$ for the LFV contribution with coupling $h_{\mu\tau}$. We neglect the electron contribution as the coupling $h_{\mu e}$ is more constrained and because of the natural hierarchy assumed in formula (6). For the charged Higgs boson we have the same coupling for the scalar and pseudoscalar contributions in the Lagrangian, therefore we give the sum of the two in one formula:

$$\Delta a_\mu^C=\frac{h_{\mu\nu}^2 m_\mu^2}{8\pi^2}\int_0^1 \frac{2x^2(x-1)}{m_\mu^2 x^2+x(m_H^2-m_\mu^2)}dx \qquad (13)$$

where we neglected terms proportional to the neutrino mass. In order to give the bounds coming from the $g-2$ measurement we chose the sets of mass and mixing angle parameters of Table I. By calculating the contribution to a_μ from the Higgs sector we obtain limits on the LFV couplings of 2HDM-III types a and b—we use only the upper limits of Eq. (11) to derive the muon $g-2$ bounds on the LFV couplings. The results are in Table II. In Fig. 2 we show the values of Δa_μ given by the 2HDM-III using the set (2) of parameters of Table I with $\lambda_{\mu\nu}=10$ as a function of $\tan\beta$. In model type a, Δa_μ is almost flat for $\tan\beta>2$, while in model type b it is a growing function of $\tan\beta$. The same is true for the other sets of parameters. In both models the Higgs sector contribution to Δa_μ is a growing function of the LFV couplings.

TABLE II. The 90% C.L. limits on the LFV couplings $\lambda_{\tau\mu}$, $\xi_{\tau\mu}$, $\eta_{\tau\mu}$ from the experimental measurement of a_μ.

Set	2HDM-III Type a	2HDM-III type b
(1)	$\lambda_{\tau\mu}<31$ ($\eta_{\tau\mu}<0.06$)	$\lambda_{\tau\mu}<6.3$ ($\xi_{\tau\mu}<0.012$)
(2)	$\lambda_{\tau\mu}<38$ ($\eta_{\tau\mu}<0.07$)	$\lambda_{\tau\mu}<0.8$ ($\xi_{\tau\mu}<0.002$)
(3)	$\lambda_{\tau\mu}<123$ ($\eta_{\tau\mu}<0.24$)	$\lambda_{\tau\mu}<2.5$ ($\xi_{\tau\mu}<0.005$)
(4)	$\lambda_{\tau\mu}<53$ ($\eta_{\tau\mu}<0.10$)	$\lambda_{\tau\mu}<5.3$ ($\xi_{\tau\mu}<0.010$)

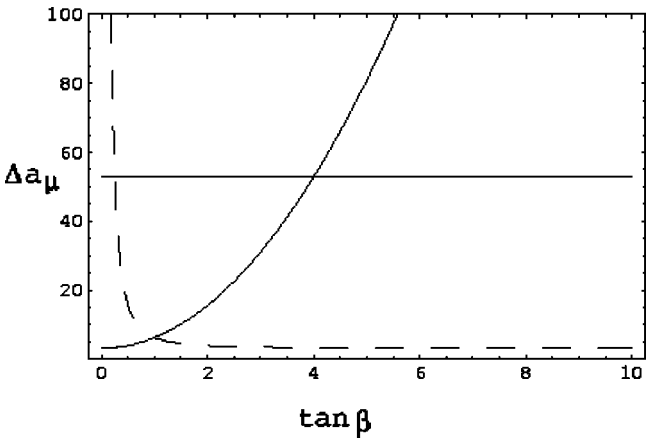

FIG. 2. Δa_μ in units of 10^{-10} as a function of $\tan\beta$ using set 2 of parameters for the 2HDM-III type a model (dashed line) and 2HDM-III type b model (continuous line). The region above the horizontal line is excluded at 90% C.L. by the muon $g-2$ data.

III. COLLIDER EXPERIMENTS

Bounds obtained from the following processes would involve two LFV couplings as in the case of $\mu\to e\gamma$: $B_s\to\mu\mu$ and $B\to X_s\mu\mu$ ($\lambda_{sb}\lambda_{\mu\mu}<9$ and $\lambda_{sb}\lambda_{\mu\mu}<4$, using 200 GeV for the scalar and the pseudo-scalar masses); $e^+e^-\to\bar{t}c\nu_e\bar{\nu}_e$; $e^+e^-\to t\bar{t}c\bar{c}$; $\mu^+\mu^-\to tc$; $B_s\to(K)\tau\mu$ and $B_s\to(K)\tau\tau$ ($\sqrt{\lambda_{sb}\lambda_{\tau\mu}}<10$); $B_s\to\tau\tau$ and $B\to K\tau\tau$ ($\sqrt{\lambda_{sb}\lambda_{\tau\mu}}<30$) [19]. The flavor changing process $t\to H^0c$ has been extensively studied for the CERN Large Hadron Collider (LHC) [28]; in the context of the 2HDM-I and -II, top quark decays beyond the SM,

$$t\to ch(h=h^0,H^0,A^0), \qquad (14)$$

were studied in [29] and it is shown that these processes could be accessible at the LHC and at the linear collider; the prospects for detecting the decay $t\to cH$ at the e^+e^- linear collider have also been investigated in [30].

The ν_μ-ν_τ flavor mixing observed in the atmospheric neutrino experiments [31] would lead to the flavor violating decays

$$\tau^\pm\to\mu^\pm\gamma, \qquad (15)$$

$$\tau^\pm\to\mu^\pm\mu^+\mu^-, \qquad (16)$$

$$\tilde{\chi}_2^0\to\tilde{\chi}_1^0\tau\mu, \qquad (17)$$

$$h\to\tau^\pm\mu^\mp. \qquad (18)$$

SUSY can accommodate the observed flavor mixing [8–10] and thus, the LFV processes (15), (16) and (17) would arise in these models. A study conducted at the LHC showed that an upper bound of 0.6×10^{-6} on the $\tau^\pm\to\mu^\pm\gamma$ branching ratio can be achieved with an integrated luminosity of 30 fb^{-1} while theoretical estimates are at the level of 10^{-9} or less [10,32]. Direct evidence of LFV in the slepton sector of SUSY would be inferred in the observation of the process (17) which has also been studied for the LHC [33]. It was

shown that in some cases, the direct evidence would offer better sensitivity than the $\tau^{\pm}\to\mu^{\pm}\gamma$ process.

The decay $h\to\tau^{\pm}\mu^{\mp}$ can be accommodated in the 2HDM-III where no discrete symmetry suppresses the LFV couplings at the tree level, and the partial decay width is parametrized by the LFV coupling $\lambda_{\tau\mu}$. The decay $H^0\to l_i^+ l_i^-$ (SM-like) will be used in the following as a comparison for the LFV decays. Its partial width is

$$\Gamma_{SM}(H^0\to l_i^+ l_i^-)=m_H\frac{1}{8\pi}\frac{m_i^2}{v^2}, \tag{19}$$

where we neglect small terms of the type m_i/m_H—see the Appendix for complete expressions. The partial width of the decay $H^0\to l_i^{\pm} l_j^{\mp}$ (where $l=e,\ \mu,\ \tau$ and $i\neq j$) is for 2HDM-III type a

$$\Gamma(H^0\to l_i^{\pm} l_j^{\mp})=m_H\frac{\lambda_{ij}^2}{8\pi}\frac{m_i m_j}{v^2}\frac{\sin^2(\alpha-\beta)}{2\sin^2\beta} \tag{20}$$

and

$$\Gamma(H^0\to l_i^{\pm} l_j^{\mp})=m_H\frac{\lambda_{ij}^2}{8\pi}\frac{m_i m_j}{v^2}\frac{\sin^2(\alpha-\beta)}{2\cos^2\beta} \tag{21}$$

for 2HDM-III type b.

Hadron colliders may be sensitive to the processes $h\to e^{\pm}\mu^{\mp}$ and $h\to\tau^{\pm}e^{\mp}$ [34], particularly at high luminosity, but these decays are not considered in the present study which is further motivated by a favorable interpretation of the atmospheric neutrino mixing experiments. It is shown in [35] that the muon collider would be sensitive to $H^0\to\tau^{\pm}\mu^{\mp}$. The non-observation of this process for $m_H<140$ GeV at the muon collider, in addition to the failure to detect the top quark decay $t\to cH^0$ at the LHC [28], would rule out the 2HDM-III [35].

In this paper we present the prospects for the detection of the LFV decay $A^0/H^0\to\tau^{\pm}\mu^{\mp}$ at the LHC and Tevatron. We shall consider the 2HDM-III and we shall parametrize the $A^0/H^0\to\tau^{\pm}\mu^{\mp}$ branching ratio (BR) by the LFV coupling parameter $\kappa_{\tau\mu}$ [36] with respect to the SM-like decay $H^0\to\tau^+\tau^-$ given in formula (19):

$$BR(A^0/H^0\to\tau\mu)=\kappa_{\tau\mu}^2\left(\frac{2m_\mu}{m_\tau}\right)BR_{SM}(H^0\to\tau\tau) \tag{22}$$

where the dependence on α, β, the ratio of the total widths and $\lambda_{\tau\mu}$ is absorbed into the LFV coupling parameter $\kappa_{\tau\mu}$. For example, for the decay and the model considered in formula (20) we have

$$\kappa_{\tau\mu}=\lambda_{\tau\mu}\frac{\sin(\alpha-\beta)}{\sqrt{2}\sin\beta}\sqrt{\frac{\Gamma_T^{SM}}{\Gamma_T^a}} \tag{23}$$

while from formula (21) we obtain

TABLE III. The correspondence between the parameters κ and λ using set 1 (set 2) of Table I for the LFV couplings of the Higgs bosons H^0 and A^0.

	$\lambda=1$	$\lambda=5$	$\lambda=10$
Type a			
$\kappa(H^0)$	1.1 (1.2)	9.4 (6.2)	7.8 (12.2)
$\kappa(A^0)$	3.3 (30.7)	16.6 (68)	7 (72.6)
Type b			
$\kappa(H^0)$	1.1 (0.7)	5 (3.3)	7.6 (6.5)
$\kappa(A^0)$	0.1 (0.001)	0.5 (0.006)	1 (0.01)

$$\kappa_{\tau\mu}=\lambda_{\tau\mu}\frac{\sin(\alpha-\beta)}{\sqrt{2}\cos\beta}\sqrt{\frac{\Gamma_T^{SM}}{\Gamma_T^b}} \tag{24}$$

where Γ_T^{SM} is the total SM-like width and $\Gamma_T^{a,b}$ is the total width in models a and b, respectively. Similar formulas can be written for the h^0 and A^0 Higgs bosons. For h^0 one has to replace $\sin(\alpha-\beta)$ in Eqs. (23) and (24) with $\cos(\alpha-\beta)$. For A^0 one has to replace $\sin(\alpha-\beta)$ with 1.

In Table III we give examples of the correspondence between the parametrization in terms of λ and the one in terms of κ for set 1 and set 2 of Table I. We shall discuss the achievable bounds on $\kappa_{\tau\mu}$ and $\lambda_{\tau\mu}$ in the following sections.

IV. SEARCH FOR $A^0/H^0\to\tau\mu$

We consider the production of the neutral Higgs bosons A^0 and H^0 through gluon fusion, $gg\to A^0/H^0$ (see Fig. 3), and the LFV decay $A^0/H^0\to\tau^{\pm}\mu^{\mp}$ (Fig. 4). We restrict the present work to the low mass region, $120<m_A<160$ GeV, primarily because the SM decay $H^0_{SM}\to\tau^+\tau^-$, hence $A^0/H^0\to\tau^+\mu^-$—see Eq. (22)—becomes negligible [37] as the SM mode $H^0_{SM}\to W^+W^-$ opens up around 160 GeV as shown in Fig. 5 where we assume $\kappa_{\tau\mu}=1$. We take as a reference the parameters of set 2 in Table I for comparison with the MSSM case without loss of generality. The events are generated in PYTHIA6.2 [38] with CTEQ5L [39] parton distribution function parametrization, and with the detector resolution and efficiencies parametrization of ATLFAST [40] from full detector simulations.

We search for a final state where the τ lepton decays to hadrons, $\tau\to$jet ν_τ with a branching ratio of $\sim$65% or to an

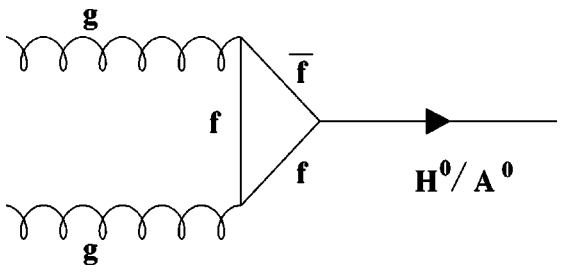

FIG. 3. Higgs boson production mechanism through gluon fusion.

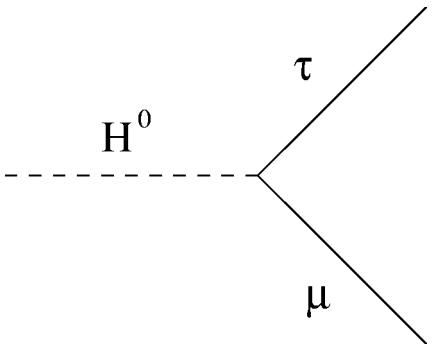

FIG. 4. The Higgs decay through the lepton flavor violating coupling $H^0\tau\mu$.

electron, $\tau\to e\nu_e\nu_\tau$ $(BR\sim 18\%)$. The main backgrounds—in both final states—include the W^+W^- pair production, the Drell-Yan type process $Z^0(\gamma^*)\to\tau^+\tau^-$. For the hadronic τ decays, an additional background comes from $W^\pm+$jets events where a jet is misidentified as a τ jet:

$$\begin{aligned} pp(\bar{p})&\to W^\pm Z^0\to\mu^\pm\nu_\mu\tau^+\tau^-,\\ &\to W^+W^-\to\mu^+\nu_\mu\tau^-\bar{\nu}_\tau,\\ &\to t\bar{t}\to\mu^\pm\nu_\mu b\tau^\mp\nu_\tau\bar{b},\\ &\to Z^0(\gamma^*)\to\tau^+\tau^-\to\mu^+\nu_\mu\bar{\nu}_\tau\tau^-,\\ &\to W^\pm+\text{jets}\to\mu^\pm\nu_\mu+\text{jets}. \end{aligned} \tag{25}$$

The $gg\to A^0/H^0$ cross sections are calculated using the program HIGLU [41]. The signal cross sections have been calculated at next-to-leading order (NLO) and next-to-next-to-leading order (NNLO) [41,42]. For the backgrounds, NLO estimates are available [43–45], except for $W^\pm+$jets where NLO calculations have been performed for a vector boson production with two jets at the Tevatron [46]. We have therefore used the leading order (LO) estimates of the signal and background cross sections. Unless explicitly stated otherwise, the normalizations of the figures referenced in Secs. IV A–IV C are that of three years at low luminosity for one experiment at the LHC using the rates shown in Table IV.

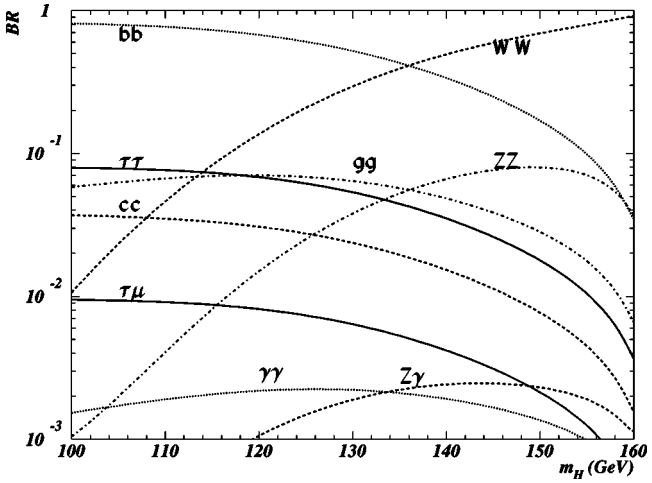

FIG. 5. The Higgs boson decay branching ratios as a function of m_H. For the $A^0/H^0\to\tau^+\mu^-+\tau^-\mu^+$ channel, the coupling parameter $\kappa_{\tau\mu}$ is taken to be one.

TABLE IV. The rates, $\sigma\times$BR(pb), for the signal $gg\to A^0/H^0\to\tau^+\mu^-+\tau^-\mu^+$, and the backgrounds at the LHC. The dominant backgrounds are $Z\to\tau\tau$ and $W^\pm+$jets where $W^\pm\to\mu^\pm\nu_\mu$ and a jet is misidentified as a τ jet. We assume the coupling parameter $\kappa_{\tau\mu}=1$ and $\tan\beta=45$ in the estimate of the signal rates. An additional background comes $gg\to A^0/H^0\to\tau^+\tau^-$ with one τ decaying to μ, $\tau\to\mu\nu_\mu\nu_\tau$ and the other τ decays to hadrons. At $\tan\beta=45$, the scalar and the pseudo-scalar Higgs bosons are degenerate in mass for $m_A\geqslant 130$ GeV, and the relative strengths of $gg\to A^0\to\tau\mu$ and $gg\to H^0\to\tau\mu$ are not important. For $m_A=120$ GeV, the A^0 and the H^0 bosons have comparable strengths.

Process	m_A (GeV)	m_H (GeV)	$\sigma\times BR$ (pb)
$gg\to A^0/H^0\to\tau^+\mu^-+\tau^-\mu^+$	119.3	128.4	7.5
	129.3	130.1	4.5
	139.2	140.2	2.1
	149.1	150.0	0.8
	159.1	160.0	0.1
$gg\to A^0/H^0\to\tau\tau$	119.3	128.4	99.5
	129.3	130.1	76.4
	139.2	140.2	54.3
	149.1	150.0	39.0
	159.1	160.0	28.5
$pp\to W^\pm Z^0\to\mu^\pm\nu_\mu\tau^+\tau^-$			0.2
$pp\to W^+W^-\to\mu^+\nu_\mu\tau^-\bar{\nu}_\tau$			1.67
$pp\to t\bar{t}\to\mu^\pm\nu_\mu b\tau^\pm\nu_\tau\bar{b}$			$1.37\ 10^1$
$pp\to Z^0(\gamma^*)\to\tau^+\tau^-\to\mu^+\nu_\mu\bar{\nu}_\tau\tau^-$			$1.39\ 10^4$
$pp\to W^\pm+\text{jets}\to\mu^\pm\nu_\mu+\text{jets}$			$1.75\ 10^4$

A. Hadronic τ decay

The event selection for the hadronic final state of the τ lepton is carried as described below:

(1) Search for one isolated muon ($p_T^\mu>20$ GeV, $|\eta^\mu|<2.5$) to provide the experimental trigger, and one hadronic τ jet ($p_T^\tau>20$ GeV, $|\eta^\tau|<2.5$). We further require a jet veto and a b-jet veto—no other jet with $p_T>20$ GeV within $|\eta|<2.5$—to reduce $W^\pm+$jets and $t\bar{t}\to\bar{b}\mu^+\nu_\mu b\tau^-\bar{\nu}_\tau$ backgrounds. A τ jet identification efficiency of 30% is assumed.

(2) The 4-momentum of the τ lepton is reconstructed from the τ jet and the missing transverse momentum (using the prescription of [47,48]) as follows:

$$\vec{p}_T{}^\tau=\vec{p}_T{}^{\tau\text{-jet}}+\vec{p}_T{}^{\text{miss}},$$

$$p_z^\tau=p_z^{\tau\text{-jet}}\left(1+\frac{p_T^{\text{miss}}}{p_T^{\tau\text{-jet}}}\right), \tag{26}$$

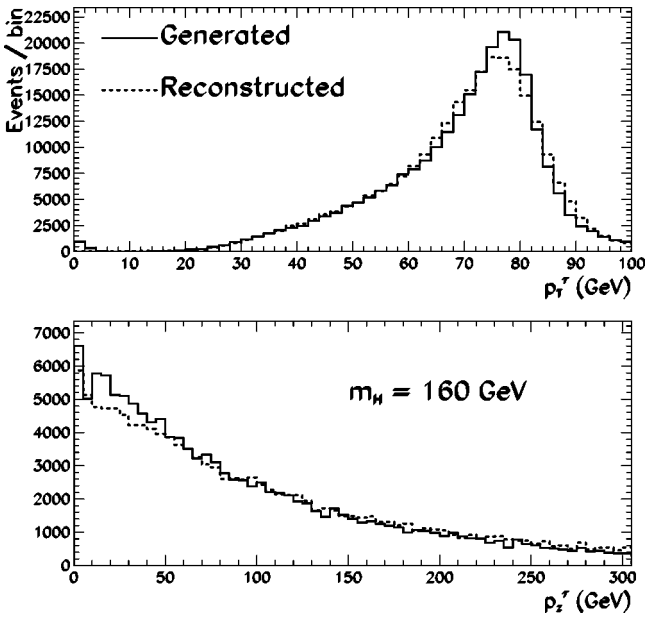

FIG. 6. The reconstructed and the generated p_T (top plot) and p_z (bottom plot) of the τ lepton. Equations (26) are used for the reconstructed quantities.

$$E_\tau^2 = \vec{p}_\tau^{\,2} + m_\tau^2.$$

The reconstructed momenta of the τ lepton using Eqs. (26) are shown in Fig. 6 together with the generated momenta. We demand that the hadronic τ jet carries at least 60% of the

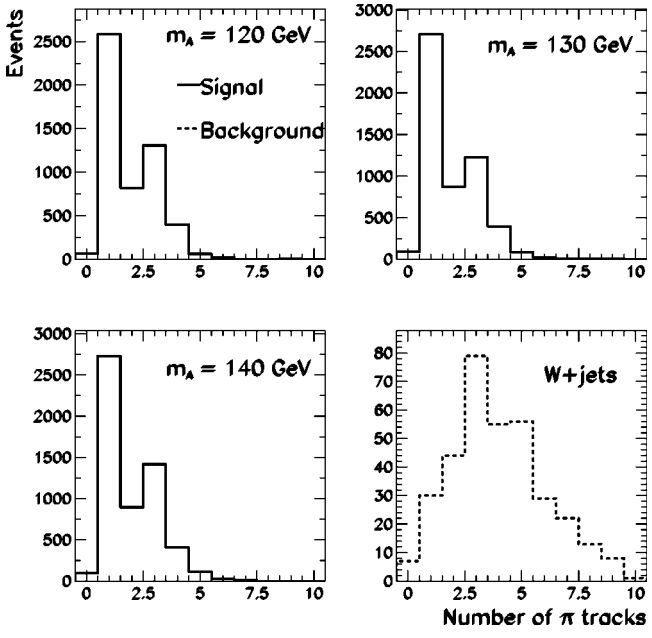

FIG. 7. The number of reconstructed charged tracks (arbitrary normalization) within $\Delta R < 0.3$ rad of the calorimeter jet axis. By requiring a single reconstructed charged track so as to select one prong τ decays, the $W^\pm$ + jets background is further reduced by one order of magnitude while the signal suffers approximately a factor of two reduction consistent with the one prong hadronic τ decay branching fraction.

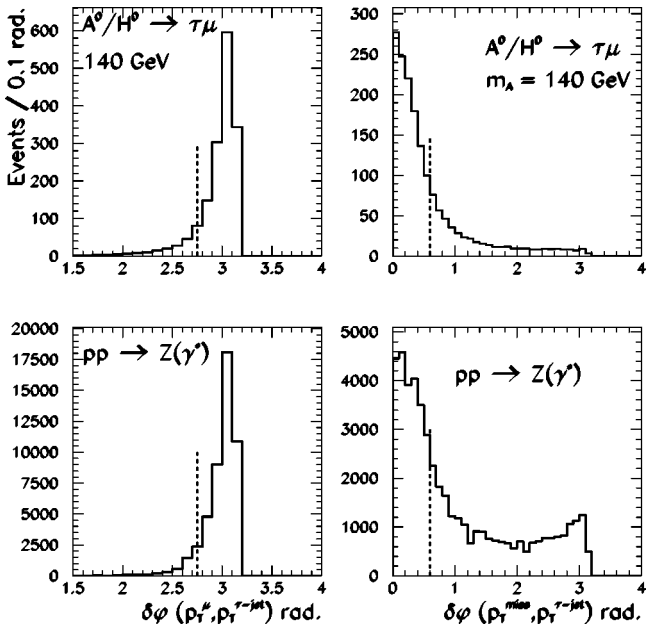

FIG. 8. The azimuthal opening angle $\delta\phi$ between the muon track and the τ jet (left plots), and between the $p_T^{\rm miss}$ vector and the τ jet (right plots). The $pp(\overline{p}) \to Z^0(\gamma^*)$ background is further reduced by a factor of two while the signal suffers only a 35% reduction. The dashed lines indicate the level of the cuts.

τ lepton energy and the cone $\Delta R = \sqrt{\Delta\eta^2 + \Delta\phi^2}$ between the τ jet axis and the τ lepton direction be less than 0.2 rad:

$$\frac{p_T^{\tau-\text{jet}}}{p_T^\tau} > 0.6,$$
$$\Delta R(p_T^{\tau-\text{jet}}, p_T^\tau) < 0.2 \ \text{rad}. \tag{27}$$

This cut reduces the background from $W^\pm$ + jets events by more than one order of magnitude while it costs only a modest $\sim$40% rejection of signal events.

(3) Using the tracker information in the off-line τ identification, we require that the τ jet candidate contains a single charged track within $\Delta R < 0.3$ rad around the jet axis. This cut would select one prong hadronic τ decay events, and as shown in Fig. 7, it reduces the $W^\pm$ + jets events by an additional factor of ten while costing only $\sim$50% reduction in the signal reconstruction efficiencies.

(4) The τ lepton from the signal is ultrarelativistic, and as a result, the missing momentum from $\tau \to (\tau\ \text{jet})\nu$ is collinear with the τ jet. Further, as a consequence of the two-body decay, the τ jet and the μ track are back to back. We therefore require a large azimuthal opening angle between the μ and the τ jet and a small opening angle between $p_T^{\rm miss}$ and the τ jet:

$$\delta\phi(p_T^\mu, p_T^{\tau\text{-jet}}) > 2.75 \ \text{rad},$$
$$\delta\phi(p_T^{\rm miss}, p_T^{\tau\text{-jet}}) < 0.6 \ \text{rad}. \tag{28}$$

As can be seen from Fig. 8, this cut reduces the signal by

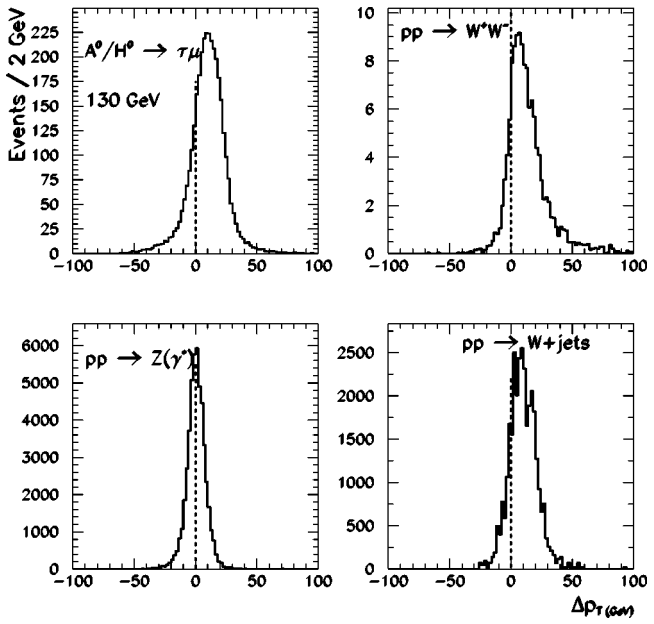

FIG. 9. The momentum imbalance Δp_T between the muon track and the τ jet. In the signal, this quantity is expected to be positive as a result of the two-body kinematics from $A^0/H^0 \to \tau^{\pm}\mu^{\mp}$ and the subsequent decay $\tau \to (\tau\,\text{jet})\nu$. This is indeed mostly the case as shown in the top left plot. Therefore, demanding $\Delta p_T > 0$ suppresses the backgrounds further, particularly the Drell-Yan type process $pp(\bar{p}) \to Z^0(\gamma^*)$, which is reduced by as much as 50% with this cut alone as can be seen from the bottom left plot.

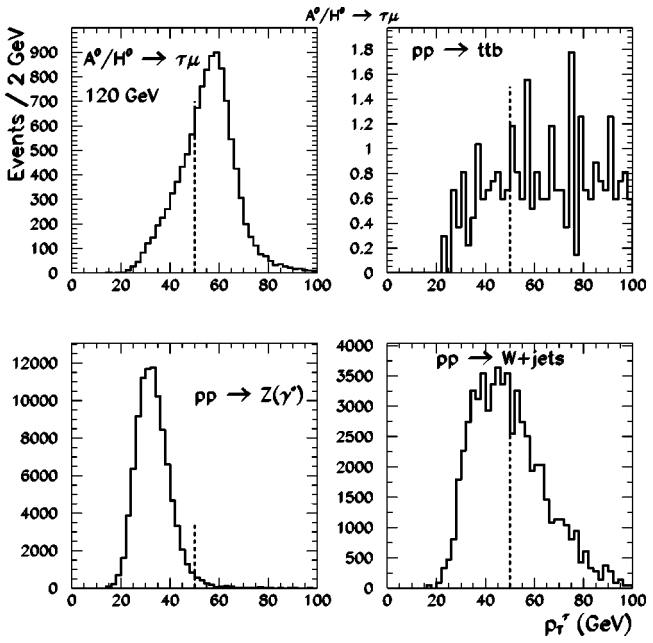

FIG. 10. The reconstructed transverse momentum of the τ lepton. We require that this quantity be greater than 50 GeV, leading to additional suppression factors of two and ten in the dominant $W^{\pm}$ + jets and $Z^0(\gamma^*) \to \tau^+\tau^-$ backgrounds, whereas the signal is reduced by at most 20%.

$\sim 35\%$ while the $pp(\bar{p}) \to Z^0(\gamma^*)$ background is further suppressed by $\sim 51\%$.

(5) The μ track is monoenergetic because of the two-body decay $H^0 \to \tau^{\pm}\,\mu^{\mp}$ but the τ jet in $\tau \to (\tau\,\text{jet})\nu$ would be somewhat softer. As a result, one would expect the momentum difference

$$\Delta p_T = p_T^{\mu} - p_T^{\tau\text{-jet}} \tag{29}$$

to be positive for the signal. Indeed, as noted in [48] and as shown in Fig. 9, this quantity is very powerful in suppressing the $pp(\bar{p}) \to Z^0(\gamma^*)$ background further.

(6) We now cut on the transverse momentum of the τ reconstructed according to Eqs. (26). The distribution of this variable is shown in Fig. 10 where one sees that demanding $p_T^{\tau} > 50$ GeV leads to at most 20% reduction in the signal—the τ gets harder at higher m_A so the reduction in the signal due to this cut is highest at the lowest mass considered, i.e., $m_A = 120$ GeV—while the $W^{\pm}$ + jets and $Z^0(\gamma^*) \to \tau^+\tau^-$ backgrounds are suppressed by additional factors of two and ten, respectively.

(7) The effective transverse mass of the $\tau\mu$ system

$$m_T = \sqrt{2 p_T^{\mu} p_T^{\tau\text{jet}} [(1 - \cos\delta\phi)]} \tag{30}$$

is reconstructed. In the signal, one would expect this quantity to peak toward the Higgs mass whereas in the backgrounds, because the final state may contain several neutrinos, the m_T distribution would peak at low values as shown in Fig. 11.

We required that $m_T > 85$ GeV. This cut suppresses the $Z^0(\gamma^*) \to \tau^+\tau^-$ background more than the other backgrounds.

The efficiencies of the cuts discussed above are shown in Table V where one sees that the analysis steps described here is effective in reducing the two main backgrounds, namely

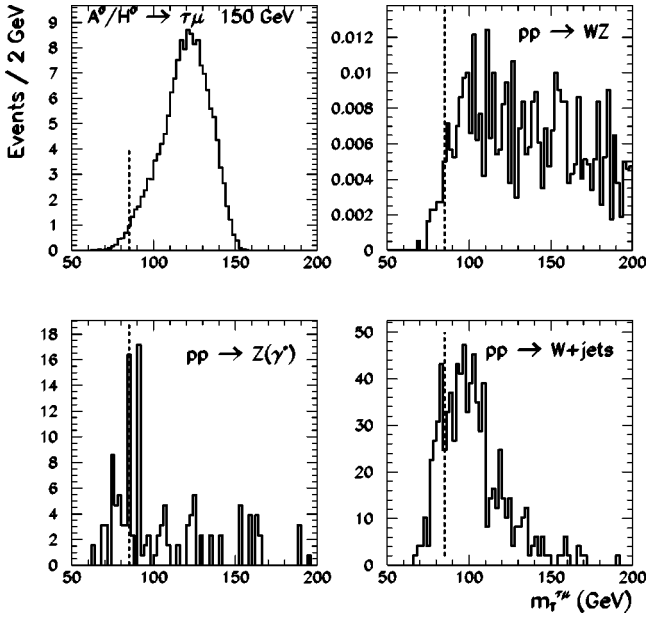

FIG. 11. The reconstructed effective transverse mass of the $\tau\mu$ system. This distribution peaks at low values in the backgrounds while in signal the peak is closer to the actual Higgs boson mass. The dashed lines indicate the cut applied on this quantity.

TABLE V. The efficiencies (in percent) of the cuts used in the current analysis. The first three cuts are effective in reducing the dominant $W^{\pm}$ + jets events while the other cuts suppress the rest of the backgrounds efficiently.

Cut	$A^0/H^0 \rightarrow \tau^{\pm}\mu^{\mp}$									
	120	130	140	150	160 GeV	$t\bar{t}$	$W^{\pm}Z^0$	W^+W^-	$Z^0(\gamma^*)$	$W^{\pm}$ + jets
(1)	16.3	17.0	16.9	17.2	20.9	3.0×10^{-1}	7.2	16.3	0.2	0.5
(2)	9.1	9.6	9.7	9.9	12.1	1.5×10^{-2}	0.50	1.3	0.09	2.2×10^{-2}
(3)	4.4	4.8	4.6	4.9	5.9	0.7×10^{-2}	0.25	0.65	0.04	2.2×10^{-2}
(4)	2.7	3.0	2.9	3.1	3.8	2.7×10^{-3}	0.10	0.40	0.02	1.9×10^{-3}
(5)	2.4	2.7	2.6	2.8	3.5	2.4×10^{-3}	0.10	0.40	0.01	1.1×10^{-3}
(6)	1.7	2.1	2.2	2.5	3.2	2.2×10^{-3}	0.05	0.20	2.4×10^{-4}	5.3×10^{-4}
(7)	1.2	2.0	2.2	2.5	3.1	2.1×10^{-3}	0.05	0.20	1.6×10^{-4}	4.3×10^{-4}

$W^{\pm}$ + jets and $Z^0 \rightarrow \tau^+\tau^-$. The most effective cuts are the ones imposed for the identification of the τ lepton—cuts (2) and (3)—and some kinematic cuts such as the momentum imbalance defined in cut (5).

With the τ 4-momentum p^{τ} obtained in Eqs. (26), the invariant mass of the Higgs boson is reconstructed,

$$m^2_{\tau\mu} = (p^{\tau} + p^{\mu})^2. \tag{31}$$

Distributions of $m_{\tau\mu}$ are shown in Fig. 12 for the signal and the backgrounds. We see in this figure that the signal is reconstructed within one GeV of the expected Higgs boson mass—except at $m_A = 120$ GeV where the A^0 and the H^0 are not degenerate in mass and their summed signal peaks somewhere in the middle—while in the backgrounds the $m_{\tau\mu}$ distribution gives a continuum spectrum dominated by $W^{\pm}$ + jets events.

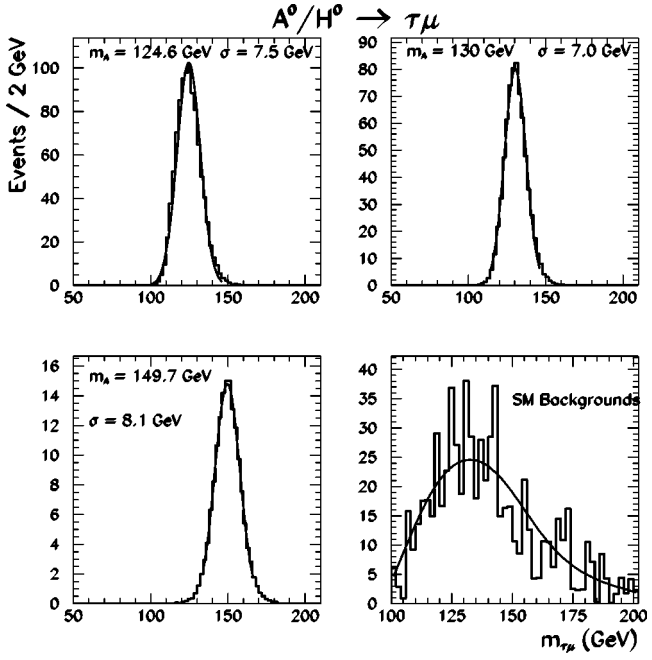

FIG. 12. The invariant mass $m_{\tau\mu}$ distributions of the signal $A^0/H^0 \rightarrow \tau^{\pm}\mu^{\mp}$ for several values of the Higgs boson mass and also of the backgrounds, after an integrated luminosity of 30 fb^{-1}. The LFV coupling parameter $\kappa^2_{\tau\mu} = 1$. The signal is reconstructed to within 5 GeV of the Higgs boson mass above the residual $W^{\pm}$ + jets continuum.

B. $A^0/H^0 \rightarrow \tau^{\pm}\mu^{\mp}$ versus $A^0/H^0 \rightarrow \tau^+\tau^-$

The $H^0 \rightarrow \tau^+\tau^-$ of the SM is not expected to yield a significant signal at the LHC due to a low signal rate and substantial backgrounds from various sources [49]. In the MSSM, for a Higgs boson of the same mass, the $A^0/H^0 \rightarrow \tau^+\tau^-$ rates are significantly larger than the SM case. The $A^0/H^0 \rightarrow \tau^+\tau^-$ process has been studied extensively for the LHC, and it is demonstrated that such a signal can be observed with a significance exceeding 5σ in a large area of the $(m_A, \tan\beta)$ plane [50,51].

The final state of both processes $A^0/H^0 \rightarrow \tau^+\tau^-$ and $A^0/H^0 \rightarrow \tau^{\pm}\mu^{\mp}$ are very similar, namely an isolated μ, a hadronic τ jet and missing energy. The observation of these signals would rely on two crucial detector performance parameters, namely a very good $p_T^{\rm miss}$ resolution and a very good τ jet identification with excellent rejection of non-τ jets. The former performance parameter is necessary for the reconstruction of the $\tau\mu$ invariant mass in $A^0/H^0 \rightarrow \tau^{\pm}\mu^{\mp}$ (as demonstrated in the above analysis) and also for the $\tau\tau$ invariant mass in $A^0/H^0 \rightarrow \tau^+\tau^-$ [50,51] while the latter performance parameter allows for the suppression of various backgrounds containing fake τ jets. We show in this section that the reconstruction procedures presented in this paper for $A^0/H^0 \rightarrow \tau\mu$ and described in [50,51] for $A^0/H^0 \rightarrow \tau\tau$ allow for the identification of each of these processes, although their final states are similar.

1. Optimization for $A^0/H^0 \rightarrow \tau\mu$

We generated $A^0/H^0 \rightarrow \tau\tau$ events and analyzed them according the analysis procedure described in Sec. IV A. The relative efficiencies of the cuts described in Sec. IV A for $A^0/H^0 \rightarrow \tau\mu$ and $A^0/H^0 \rightarrow \tau\tau$ final states are shown in Table VI. From Fig. 13 we see that at the same Higgs boson mass, the reconstructed $\tau\mu$ invariant mass for the $A^0/H^0 \rightarrow \tau^+\tau^-$ events peaks at lower values.

2. Optimization for $A^0/H^0 \rightarrow \tau\tau$

It is also important to show that the analysis technique optimized for the search for the $A^0/H^0 \rightarrow \tau\tau$ signal is capable

TABLE VI. The relative efficiencies (in percent) of the cuts used in the current analysis for $A^0/H^0 \to \tau\tau$ events, to be compared to Table V where the efficiencies for $A^0/H^0 \to \tau\mu$ are shown.

Cut	$A^0/H^0 \to \tau\tau$				
	120	130	140	150	160 GeV
(1)	2.0	4.2	2.1	1.95	1.77
(2)	0.6	1.1	0.6	0.52	0.47
(3)	0.3	0.6	0.3	0.26	0.23
(4)	0.1	0.24	0.12	0.11	0.10
(5)	0.09	0.18	0.09	0.08	0.08
(6)	0.01	0.04	0.02	0.03	0.03
(7)	0.8×10^{-2}	0.02	0.02	0.02	0.03

of separating the $\tau\tau$ final state from the $\tau\mu$ events. We have therefore examined $A^0/H^0 \to \tau\mu$ events according to the $A^0/H^0 \to \tau\tau$ analysis technique which we recall succinctly as follows [50,51]:

(a) One isolated μ with $p_T > 24$ GeV and $|\eta| < 2.5$, one hadronic τ jet with $E_T^{jet} > 40$ and $|\eta| > 2.5$ and b-jet veto.

(b) $E_T^{miss} > 18$ GeV.

(c) The transverse mass $m_T(\text{lepton-}E_T^{miss}) < 25$ GeV.

(d) $1.8 < \Delta\phi < 2.9$ rad or $3.4 < \Delta\phi < 4.9$ rad, where $\Delta\phi$ is the azimuthal opening angle between the τ jet and the isolated μ. This cut is needed for the reconstruction of the $\tau\tau$ invariant mass $m_{\tau\tau}$. Indeed, the invariant mass $m_{\tau\tau}$ of the pair of τ leptons produced in the process

$$A^0/H^0 \to \tau\tau \to \text{jet}\ \ \nu_\tau \mu \nu_\mu \nu_\tau$$

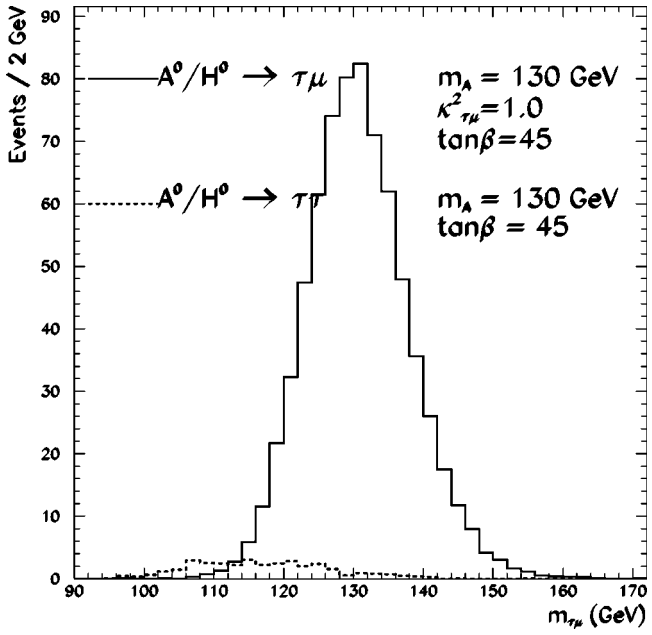

FIG. 13. The reconstructed $m_{\tau\mu}$ invariant mass for $A^0/H^0 \to \tau\mu$ and $A^0/H^0 \to \tau^+\tau^-$ $m_A = 130$ GeV and $\kappa_{\tau\mu} = 1$ ($\tan\beta = 45$, $\alpha = -0.58$ rad), i.e. set 2 of Table I using the analysis procedure presented above. The existence of the $A^0/H^0 \to \tau^+\tau^-$ signal would constitute an additional background for the $A^0/H^0 \to \tau^\pm\mu^\mp$ process.

TABLE VII. The relative efficiencies (in percent) of the cuts used in the search for $A^0/H^0 \to \tau\tau$ [50,51] and restated briefly in the text ($m_A = 130$ GeV).

Cut	$A^0/H^0 \to \tau^\pm\mu^\mp$	$A^0/H^0 \to \tau\tau$
(a)	15.1	3.1
(b)	5.3	1.9
(c)	0.2	1.5
(d)	0.02	0.3

can be reconstructed assuming that $m_\tau = 0$, that the τ detected products (in this case the τ jet and the μ) are not back to back, and also that the direction of the neutrino system from each τ decay coincides with that of the detected product:

$$m_{\tau\tau} = \sqrt{2(E_1 + E_{\nu 1})(E_2 + E_{\nu 2})(1 - \cos\theta)}. \qquad (32)$$

E_1 and E_2 are the visible energies from the τ decays, θ is the angle between the directions of the detected products, and $E_{\nu 1}$ and $E_{\nu 2}$ are the energies of the two neutrino systems, obtained by solving the system of equations

$$p_x^{miss}(p_y^{miss}) = [E_{\nu 1}\overline{u}_1]_{x(y)} + [E_{\nu 2}\overline{u}_2]_{x(y)},$$

where $\overline{u}_1$ and $\overline{u}_1$ are the directions of the detected products, and p_x^{miss} and p_y^{miss} the components of the E_T^{miss} vector. The above system of equations can be solved if the determinant, which is proportional to $\sin\Delta\phi$, is not zero. Further details of the $m_{\tau\tau}$ reconstruction are well documented elsewhere [50,51].

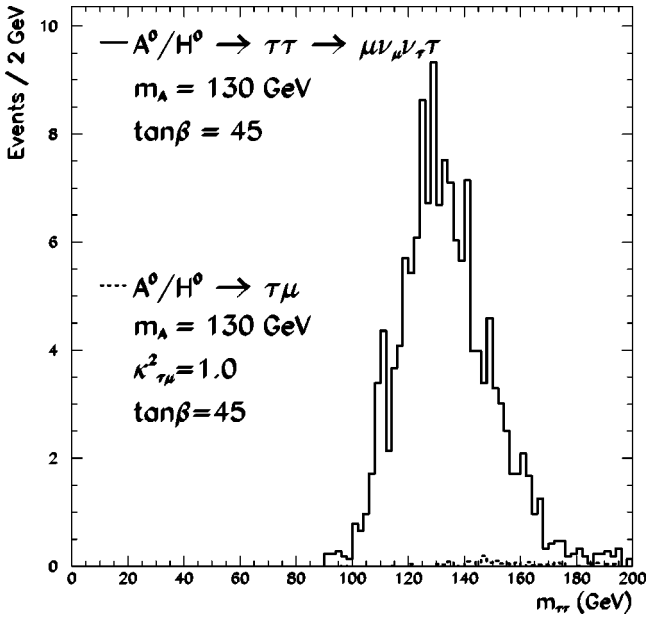

FIG. 14. The reconstructed $m_{\tau\tau}$ invariant mass for $A^0/H^0 \to \tau\tau$ and $A^0/H^0 \to \tau\mu$, for $m_A = 130$ GeV and $\kappa_{\tau\mu} = 1$ ($\tan\beta = 45$, $\alpha = -0.58$ rad), i.e. set 2 of Table I using the analysis procedure presented in [50,51]. The existence of the $A^0/H^0 \to \tau\mu$ signal would constitute a negligible background for the $A^0/H^0 \to \tau\tau$ process.

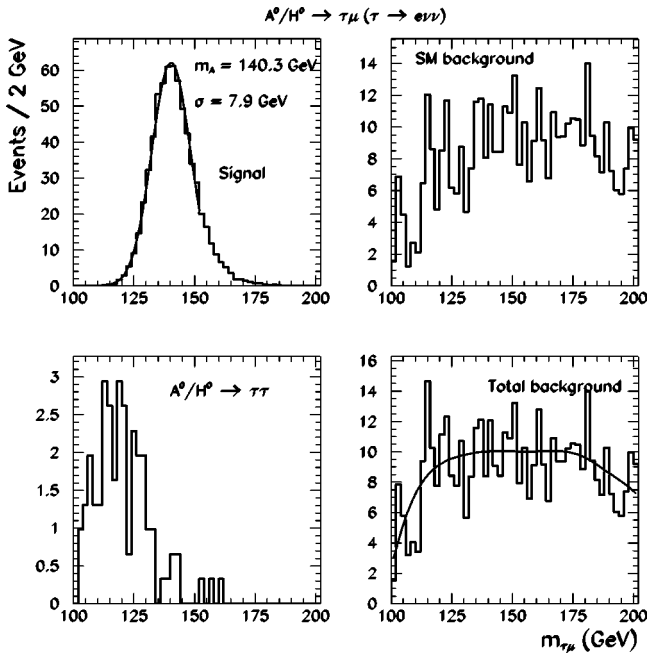

FIG. 15. The reconstructed invariant mass $m_{\tau\mu}$ in the leptonic decay of the τ ($\rightarrow e\nu\nu$) for the signal ($m_A=140$ GeV, $\tan\beta=45$, $\kappa=1$), the SM backgrounds and the $A^0/H^0\rightarrow\tau\tau$ background.

The relative efficiencies of the cuts (a)–(d) for the $\tau\mu$ and $\tau\tau$ final states are shown in Table VII. Figure 14 shows the reconstructed $m_{\tau\tau}$ invariant mass distribution for both final states. The $\tau\mu$ events would contribute a negligible background under the $\tau\tau$ signal.

The reconstruction procedure for $A^0/H^0\rightarrow\tau^+\tau^-$ described in [50,51] and the analysis steps presented above for $A^0/H^0\rightarrow\tau^{\pm}\mu^{\mp}$ would allow for the separation of both signals, with each contributing a small residual background under the peak of the other as shown in Figs. 13 and 14.

TABLE VIII. The rates, $\sigma\times BR$(pb), for the signal $gg\rightarrow A^0/H^0\rightarrow\tau^+\mu^-+\tau^-\mu^+$, and the backgrounds at the Tevatron. We assume $\kappa_{\tau\mu}=1$ and $\tan\beta=45$.

Process	m_A (GeV)	m_H (GeV)	$\sigma\times$BR (pb)
$gg\rightarrow A^0/H^0\rightarrow\tau^+\mu^-+\tau^-\mu^+$	119.3	128.4	1.41×10^{-1}
	129.3	130.1	0.79×10^{-1}
	139.2	140.2	0.33×10^{-1}
	149.1	150.0	0.11×10^{-1}
	159.1	160.0	0.15×10^{-2}
$gg\rightarrow A^0/H^0\rightarrow\tau\tau$	119.3	128.4	3.90
	129.3	130.1	2.84
	139.2	140.2	1.79
	149.1	150.0	1.16
	159.1	160.0	0.75
$p\bar{p}\rightarrow Z^0(\gamma^*)\rightarrow\tau^+\tau^-\rightarrow\mu^+\nu_\mu\bar{\nu}_\tau\tau^-$		3.24×10^3	
$p\bar{p}\rightarrow W^{\pm}+\text{jets}\rightarrow\mu^{\pm}\nu_\mu+\text{jets}$		3.21×10^3	

TABLE IX. The expected signal-to-background ratios and signal significances ($\tau\rightarrow$jet $\nu/\tau\rightarrow e\nu\nu$) for two experiments at the Tevatron, assuming $\kappa^2_{\tau\mu}=1$ and 5% systematic uncertainty on the background shape and normalization.

m_A (GeV) $\rightarrow$	120	130	140	150
Signal (S)	10/29	7/19	3/13	1/5
Backgrounds (B)	4/42	4/44	3/51	2/62
S/B	2.4/0.7	1.8/0.4	1.0/0.3	0.5/0.1
$S/\sqrt{B}$	5.0/4.3	3.5/2.7	1.7/1.7	1.2/0.6
Combined $S/\sqrt{B}$	6.6	4.4	2.4	1.3

C. Leptonic τ decay

Thus far, we have considered the hadronic final state of the τ lepton, and the major irreducible background comes from $W+$jets events where a jet is mis-identified as a hadronic τ jet. Indeed, the residual SM background shown in Fig. 12 is dominated by $W+$jets events whose rate is several orders of magnitude higher than the signal rates as shown in Table IV. In this section we examine the leptonic decay of the τ, namely $\tau\rightarrow e\nu_e\bar{\nu}_\tau$. Although the branching fraction of $\tau\rightarrow e\nu_e\bar{\nu}_\tau$ is only $\sim$18% compared to 65% for $\tau\rightarrow(jet)\nu_\tau$, the identification of the electron is easier with an efficiency of 90% whereas the τ jet identification efficiency is much lower: in the above analysis, we assume a τ jet identification efficiency of 30%, corresponding to a jet rejection factor of $\sim$400—see [50] for details.

Furthermore, the leptonic decay of the τ will not be sensitive to the $W+$jets background. We search for a signal final

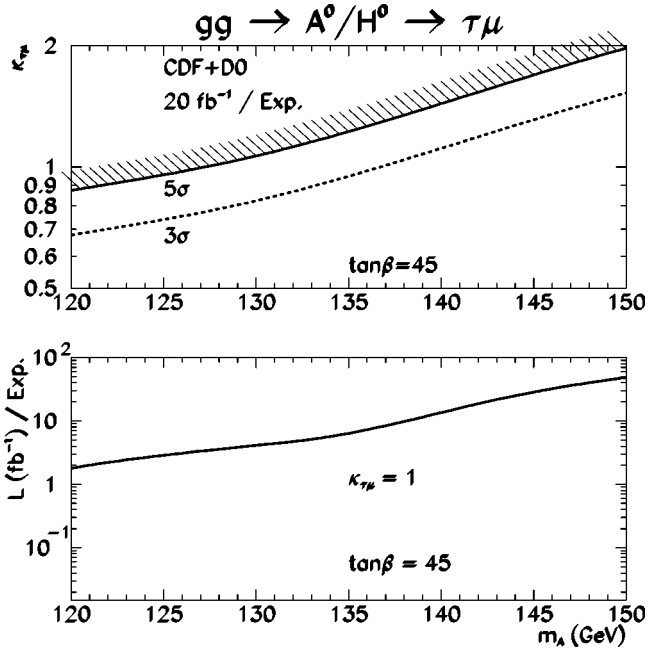

FIG. 16. The discovery reach at the Tevatron in the combined $\tau\rightarrow$jet ν_τ and $\tau\rightarrow e\nu_e\nu_\tau$ channels. The signal would yield a 5σ significance for $0.87\lesssim\kappa_{\tau\mu}\lesssim2.0$ and for a Higgs boson mass $120\lesssim m_A\lesssim150$ GeV. The luminosity needed for a 95% C.L. exclusion is shown in the bottom plot.

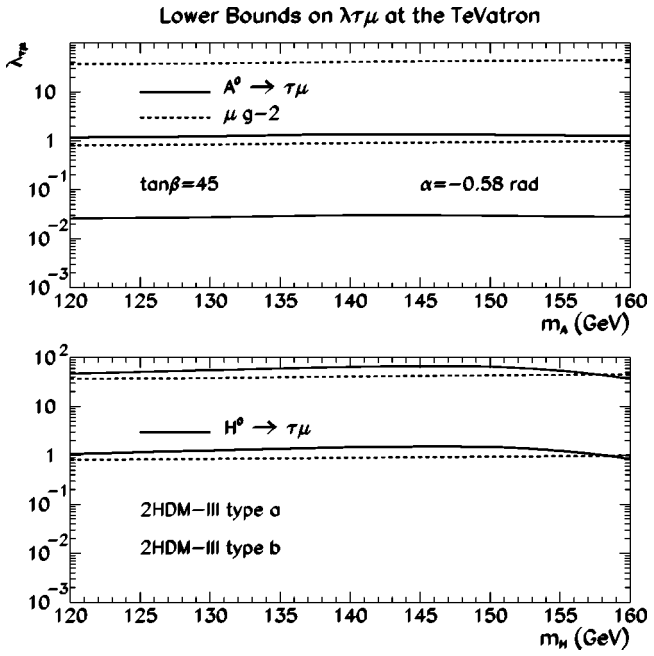

FIG. 17. The achievable lower bounds on the LFV coupling $\lambda_{\tau\mu}$ at the Tevatron (CDF+D0) obtained from the summed signal in the hadronic and leptonic decays of the τ lepton. To obtain these bounds, we use the values of $\kappa_{\tau\mu}$ at 5σ shown in Fig. 16—20 fb^{-1} per experiment. The current bounds on $\lambda_{\tau\mu}$ obtained from the muon $g-2$ data are also shown. For the muon $g-2$ data, the curves at higher $\lambda_{\tau\mu}$ values correspond to the 2HDM-III type a and the lower curves to the 2HDM-III type b. This trend is the same for $H^0 \to \tau\mu$ (bottom plot) but it is reversed for $A^0 \to \tau\mu$ (top plot).

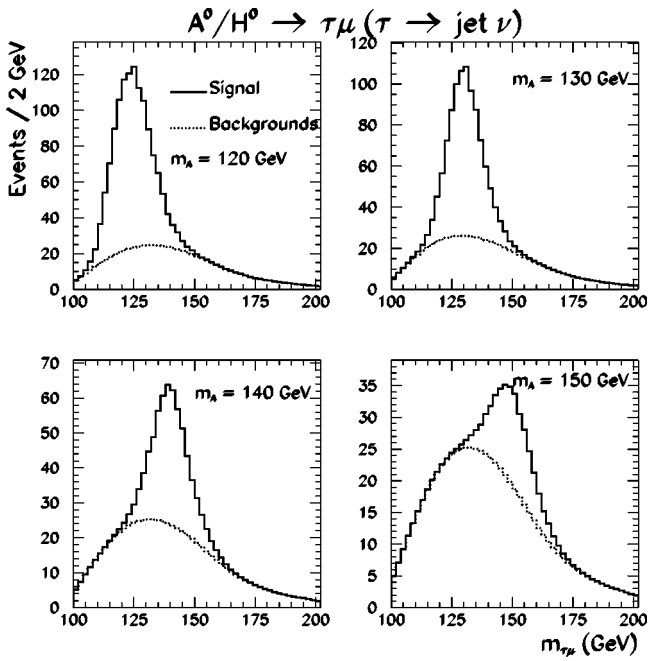

FIG. 18. The reconstructed invariant mass $m_{\tau\mu}$, after cut (7), of the signal plus the backgrounds in the hadronic τ decay channel for $m_A = 120$, 130, 140 and 150 GeV, and for an integrated luminosity of 30 fb^{-1} at the LHC. For the assumed value of the LFV coupling parameter ($\kappa^2_{\tau\mu}=1$), the signal can be observed with a significance exceeding 5σ up to $m_A = 150$ GeV.

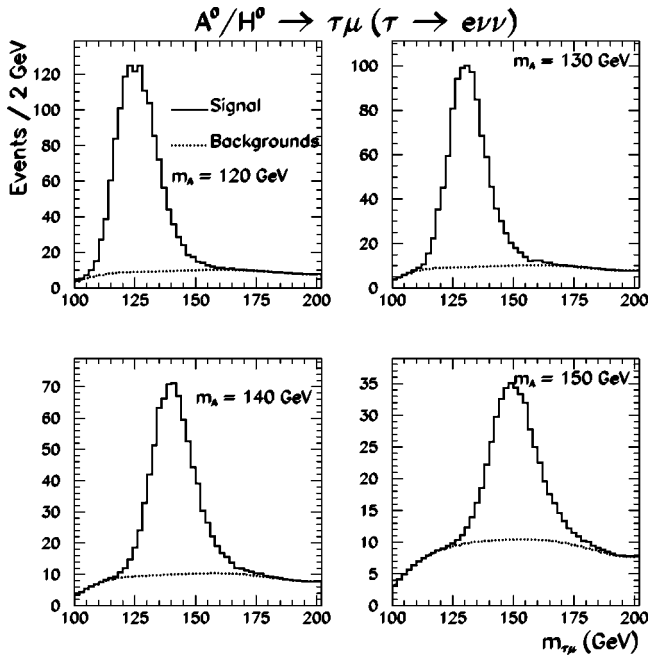

FIG. 19. The same as Fig. 18 but with the leptonic decay of the τ ($\to e\nu_e\nu_\tau$).

state containing two isolated leptons, one electron and the other a μ with no hadronic activity. The major SM backgrounds in this case are shown in Table IV—the processes listed in Eq. (25)—except for the W+jets background, in addition to

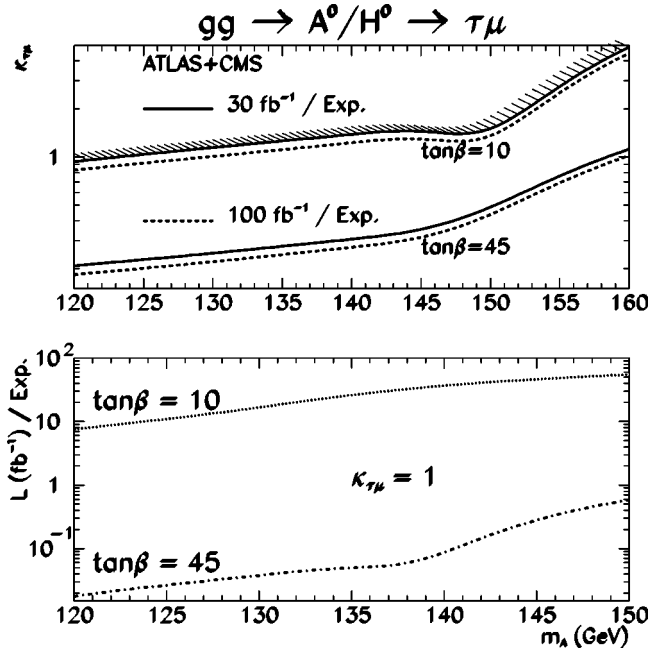

FIG. 20. The 5σ discovery reach in the (m_A, $\kappa_{\tau\mu}$) plane, using the combined $\tau \to$ jet ν_τ and $\tau \to e\nu_e\nu_\tau$ signals, for ATLAS + CMS (top plot). The $A^0/H^0 \to \tau^\pm\mu^\mp$ signal would yield a 5σ significance for $0.18 \lesssim \kappa_{\tau\mu} \lesssim 1.0$ and for a Higgs boson mass $120 \lesssim m_A \lesssim 160$ GeV. The bottom plot shows the luminosity needed for a 95% C.L. exclusion as a function of m_A for low and high $\tan\beta$ assuming $\kappa_{\tau\mu}=1$.

TABLE X. The signal-to-background ratios and signal significances calculated within $\pm 2\sigma$ of the reconstructed Higgs boson mass $\langle m_A \rangle$ for $\tau \to$ jet $\nu/\tau \to e\nu\nu$—one experiment at the LHC—with an integrated luminosity of 30 fb^{-1}, assuming $\kappa^2_{\tau\mu}=1$ and 5% systematic uncertainty from the residual background shape and normalization.

m_A (GeV) $\to$	120	130	140	150	160
$\langle m_A \rangle$ (GeV)	124.6/125.2	130.0/130.7	139.9/140.6	149.7/150.0	159.4/159.8
σ (GeV)	7.5/7.3	7.0/7.0	7.6/8.2	8.1/9.1	8.4/10.4
Signal (S)	943/1142	687/816	349/624	144/279	23/57
Backgrounds (B)	360/134	397/140	376/163	296/198	223/226
S/B	2.6/8.5	1.7/5.8	0.9/3.8	0.5/1.4	0.1/0.3
$S/\sqrt{B}$	36.1/85.4	24.4/59.4	12.9/41.2	6.3/16.2	1.2/3.0
Combined $S/\sqrt{B}$	92.7	64.2	43.2	17.4	3.2

$$t\bar{t} \to \mu\nu_\mu b e \nu_e \bar{b}, \qquad WW \to \mu\nu_\mu e \nu_e . \tag{33}$$

The reconstruction of the signal is exactly as described in Sec. IV A, except for the cuts (2) and (3) which were implemented for the suppression of the $W+$jets events and for the selection of the one prong hadronic τ decays. These cuts are no longer necessary and are not used in the search for the leptonic decay of the τ. Fig. 15 shows the reconstructed $\tau\mu$ invariant mass for the signal $A^0/H^0 \to \tau\mu$, the SM backgrounds and for the $A^0/H^0 \to \tau\tau$ background with one τ decaying to leptons: $\tau \to e\nu\nu$. In this channel, too, the signal can be observed with significances exceeding 5σ, depending on the LFV coupling parameter $\kappa_{\tau\mu}$.

D. Prospects at the Tevatron

Table VIII shows the estimated signal and background rates at the Tevatron where we propose to search for $A^0/H^0 \to \tau^\pm \mu^\mp$ with the neutral Higgs bosons of the 2HDM produced through gluon fusion: $gg \to A^0/H^0$. The signal-to-background ratios and the signal significances calculated within $\pm 2\sigma$ of the reconstructed Higgs mass peak, for an integrated luminosity of 20 fb^{-1} per experiment, are shown in Table IX for $\kappa^2_{\tau\mu}=1$ and $\tan\beta=45$. At the Tevatron, a significant signal ($>5\sigma$) can be detected for Higgs boson masses around 120 GeV and high $\tan\beta$ (~ 45), assuming $\kappa_{\tau\mu} \sim 1$. We show in Fig. 16 the discovery reach at the Tevatron and the luminosity required for a 95% confidence level exclusion for large $\tan\beta$. For low $\tan\beta$ values ($\lesssim 10$), the signal production rate decreases by more than an order of magnitude compared to the case shown in Table VIII so that the detection of this process at the Tevatron would require very large values of the LFV coupling $\lambda_{\tau\mu}$. However, one would expect the LFV couplings $\lambda_{ij} \sim \mathcal{O}(1)$ [35,48]—see Eqs. (23) and (24). Therefore, at the Tevatron, this channel would be viable only in the event of a large $\tan\beta$ value and for $\kappa_{\tau\mu} \sim 1$—see Table III for the correspondence between $\kappa_{\tau\mu}$ and $\lambda_{\tau\mu}$. Figure 17 shows the corresponding expected limits on $\lambda_{\tau\mu}$ at the Tevatron: the reach in $\lambda_{\tau\mu}$ would be extended, at large $\tan\beta$, beyond that obtained from the muon $g-2$ experiment, for $A^0 \to \tau\mu$ in the 2HDM-III type a.

As shown in Fig. 17, the bounds on $\lambda_{\tau\mu}$ would be different for the Higgs bosons A^0, H^0 and h^0 because of their different LFV Yukawa couplings—see Secs. II and III and the Appendix.

E. Prospects at the LHC

The signal and background rates at the LHC are shown in Table IV. In Figs. 18 and 19 we show the reconstructed $m_{\tau\mu}$ invariant mass for several values of the Higgs boson mass, and for an integrated luminosity of 30 fb^{-1}, and for the LFV coupling parameter $\kappa^2_{\tau\mu}=1$.

The signal-to-background ratios and the signal significances are calculated with the events reconstructed within $\pm 2\sigma$

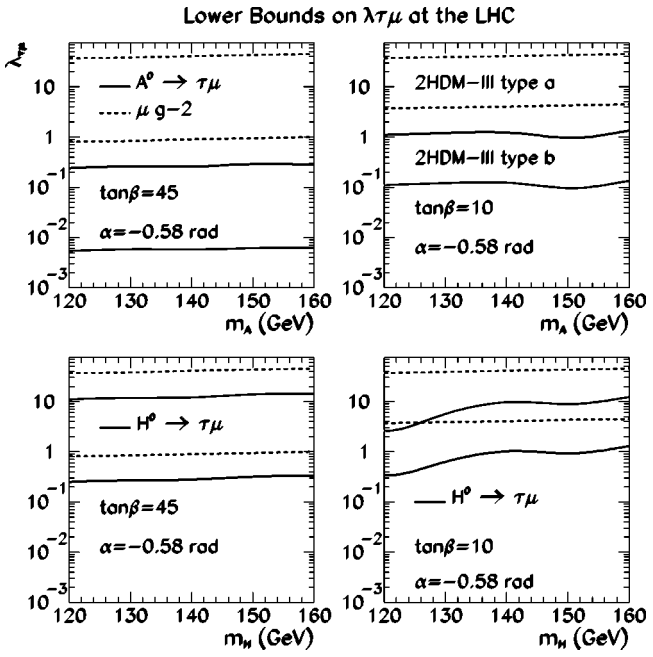

FIG. 21. The achievable bounds on the LHV coupling $\lambda_{\tau\mu}$ at the LHC (ATLAS + CMS) from the combined hadronic and leptonic τ decay channels—100 fb^{-1} per experiment. For low or high $\tan\beta$, the lower bounds on $\lambda_{\tau\mu}$ at the LHC would be extended beyond that of the muon $g-2$ experiment. For the muon $g-2$ data, the curves at higher $\lambda_{\tau\mu}$ values correspond to the 2HDM-III type a and the lower curves to the 2HDM-III type b. This trend is the same for $H^0 \to \tau\mu$ (bottom plots) but it is reversed for $A^0 \to \tau\mu$ (top plots).

of the reconstructed Higgs boson mass. As shown in Table X, a significant signal can be observed at the LHC for Higgs masses in the range 120 to 150 GeV for the LFV coupling parameter $\kappa_{\tau\mu} \sim \mathcal{O}(1)$. Around 160 GeV, as the $H^0_{SM} \rightarrow W^+W^-$ channel opens up, the rate for $A^0/H^0 \rightarrow \tau^\pm \mu^\mp$ decreases so drastically that the observation of a significant signal would be possible only in the event of $\kappa_{\tau\mu} > 1$.

The constraints on this LFV coupling $\lambda_{\tau\mu}$ from low energy experiments are rather weak—see the discussion in Sec. II on low energy bounds. From Eq. (22) the signal rate scales like $\kappa^2_{\tau\mu}$ and we show in Fig. 20 the value of $\kappa_{\tau\mu}$ at which the signal yields a 5σ significance around the Higgs boson mass peak. The LFV coupling $0.18 \lesssim \kappa_{\tau\mu} \lesssim 1.0$ can be reached at the LHC, combining ATLAS and CMS data for Higgs boson masses $120 \lesssim m_A \lesssim 160$ GeV. Fig. 20 also shows in the bottom plot, the luminosity needed at the LHC to achieve a 2σ (95% C.L.) exclusion. At the LHC, assuming the LFV coupling parameter $\kappa_{\tau\mu} \sim \mathcal{O}(1)$, a few years of low luminosity data would be enough to exclude this model in the mass range $120 < m_A < 150$ GeV and at low $\tan\beta$. For high $\tan\beta$ values, a 95% C.L. exclusion can be established in one year of data taking or less for the mass range considered. In Fig. 21 we show the expected bounds on $\lambda_{\tau\mu}$ at the LHC using the values of $\kappa_{\tau\mu}$ at 5σ from Fig. 20 and we see that the reach in $\lambda_{\tau\mu}$ would be extended beyond the muon $g-2$ limits.

V. CONCLUSIONS

In models with several Higgs doublets, FCNC and LFV couplings exist at the tree level because the diagonalization of the up-type and the down-type mass matrices does not ensure the diagonalization of the Higgs-fermion coupling matrices. In the 2HDM-I and -II, a discrete symmetry suppresses FCNC and LFV couplings at the tree level by restricting fermions of a given electric charge to couple to at most one Higgs doublet. In the 2HDM-III, no discrete symmetry is invoked and the flavor changing couplings are parametrized in terms of the fermion mass hierarchy to be in agreement with the severe experimental constraints on FCNC and LFV couplings with the first generation index. The arbitrariness of the FCNC and LFV couplings of the second and the third generations can be constrained in low energy and collider experiments. The deviation of the measured muon anomalous magnetic moment from the SM prediction offers weak bounds on the LFV coupling parameter $\lambda_{\tau\mu}$.

We have investigated the achievable bound on $\kappa_{\tau\mu}$ and $\lambda_{\tau\mu}$ at hadron colliders by studying the $gg \rightarrow A^0/H^0 \rightarrow \tau^\pm \mu^\mp$ signal observability. Considering the hadronic decay of the τ lepton, the main backgrounds of this process are $Z^0(\gamma) \rightarrow \tau^+\tau^-$ and $W^\pm$+jets events where $W^\pm \rightarrow \mu^\pm \nu_\mu$ and a jet is misidentified as a τ jet. We search for an isolated μ and one τ jet, and we applied a jet veto and a b-jet veto to reject multi-jet final states from $t\bar{t}$ and $W^\pm$+jets. Further reduction of the backgrounds is achieved by exploiting the differences in the event topology of the signal and the various backgrounds. Although the background rates are several orders of magnitude higher than the signal rate, three main detector performance parameters have been crucial in extracting a significant signal: a good τ jet identification and rejection against non-τ jets, the tracking capability for the identification of the charged tracks in one prong hadronic τ decays, and the missing momentum resolution.

We also investigated the leptonic decay of the τ ($\rightarrow e\nu\nu$) where the W+jets event do not contribute a significant background. In this case we require a final state containing one isolated μ and one isolated electron, and we use jet veto and b-jet veto to suppress the $t\bar{t}$ background. The leptonic decay of the τ gives a better sensitivity. The signal significances are estimated based on expected events in both the hadronic and the leptonic τ decay channels.

The analysis steps described above reconstruct the $\tau\mu$ invariant mass to within ~ 1 GeV of the Higgs boson mass (except at $m_A = 120$ GeV where the A^0 and the H^0 bosons are not degenerate and the summed signal peaks somewhere in the middle as a result), and also differentiate the $A^0/H^0 \rightarrow \tau^+\tau^-$ events from the $A^0/H^0 \rightarrow \tau^\pm\mu^\mp$ signal.

With an integrated luminosity of 20 fb^{-1} at the Tevatron, a signal for $0.87 \lesssim \kappa_{\tau\mu} \lesssim 2.0$ could be detected with a significance of 5σ for Higgs boson masses $120 \lesssim m_A \lesssim 150$ GeV, corresponding to a reach in $\lambda_{\tau\mu}$ of the order 0.03/1.0 for the 2HDM-III type a/type b. In case the signal is not observed and assuming $\kappa_{\tau\mu} \sim \mathcal{O}(1)$, a 95% C.L. exclusion can be set with < 14 fb^{-1} of data for $120 \lesssim m_A \lesssim 140$ GeV.

The sensitivity will be improved at the LHC where $\kappa_{\tau\mu} \sim 0.18$ could be reached with 100 fb^{-1}—this would correspond to a lower bound in $\lambda_{\tau\mu} \sim 0.01/0.1$ for the 2HDM-III type a/type b. A 95% C.L. exclusion could be set after just a few years of running at low luminosity if the signal is not observed.

At the LHC, the reach in the LFV coupling $\lambda_{\tau\mu}$ would be extended beyond that expected at the Tevatron and also beyond that obtained from the muon $g-2$ data: a factor of 10 to 100 better, depending on $\tan\beta$ and α.

ACKNOWLEDGMENTS

This work was partially performed within the ATLAS Collaboration and we thank collaboration members for helpful comments. We have used the physics analysis framework and tools which are the results of the collaboration's wide efforts. The authors would like to thank E. Richter-Wąs and G. Azuelos for discussions and comments, and also to T. Sjöstrand for helpful correspondence.

APPENDIX

In this appendix we give the Lagrangian of the lepton flavor conserving and violating Yukawa couplings of the 2HDM type III using the results of [52] with the addition of the charged Higgs part. The leptonic Yukawa Lagrangian reads

$$-\mathcal{L} = \eta_{ij} \overline{l^0_{iL}} \varphi_1 l^0_{jR} + \xi_{ij} \overline{l^0_{iL}} \varphi_2 l^0_{jR} + \text{H.c.} \qquad \text{(A1)}$$

where $\varphi_{1,2}$ are the two Higgs doublets

$$\varphi_1=\begin{pmatrix}\phi_1^+\\ \phi_1^0\end{pmatrix},\quad \varphi_2=\begin{pmatrix}\phi_2^+\\ \phi_2^0\end{pmatrix} \tag{A2}$$

with vacuum expectation values

$$\langle\varphi_1\rangle_0=\frac{1}{\sqrt{2}}\begin{pmatrix}0\\ v_1\end{pmatrix},\quad \langle\varphi_2\rangle_0=\frac{1}{\sqrt{2}}\begin{pmatrix}0\\ v_2 e^{i\theta}\end{pmatrix}, \tag{A3}$$

where in the following we set $\theta=0$ and therefore we consider a *CP*-conserving Higgs sector. The parameters η_{ij} and ξ_{ij} are non-diagonal 3×3 matrices and i, j are family indices. The neutral and charged mass eigenstates are related to the states of Eq. (A2) by

$$\begin{pmatrix}\cos\beta & -\sin\beta\\ \sin\beta & \cos\beta\end{pmatrix}\begin{pmatrix}G_W^\pm\\ H^\pm\end{pmatrix}=\begin{pmatrix}\phi_1^\pm\\ \phi_2^\pm\end{pmatrix}$$

$$\begin{pmatrix}\cos\beta & -\sin\beta\\ \sin\beta & \cos\beta\end{pmatrix}\begin{pmatrix}G_Z^0\\ A^0\end{pmatrix}=\sqrt{2}\begin{pmatrix}\Im\phi_1^0\\ \Im\phi_2^0\end{pmatrix} \tag{A4}$$

$$\begin{pmatrix}\cos\alpha & -\sin\alpha\\ \sin\alpha & \cos\alpha\end{pmatrix}\begin{pmatrix}H^0\\ h^0\end{pmatrix}=\sqrt{2}\begin{pmatrix}\Re\phi_1^0-v_1/\sqrt{2}\\ \Re\phi_2^0-v_2/\sqrt{2}\end{pmatrix}$$

where $\Re\phi$ and $\Im\phi$ are the real and imaginary parts of the complex scalar fields ϕ, $\tan\beta=v_2/v_1$, α is the *CP*-even neutral Higgs sector mixing angle, G_Z^0 and $G_W^\pm$ are the would-be Goldstone bosons of Z and W vector bosons, and $H^\pm$, A^0, H^0, h^0 are the physical Higgs bosons of the 2HDM. The Lagrangian (A1) in terms of the mass eigenstates is obtained by a unitary transformation

$$l_{L,R}=V_{L,R}\ \ l_{L,R}^0 \tag{A5}$$

and one can write the diagonal mass matrix for the three leptons

$$M_l^{\rm diag}=V_L\left(\frac{v_1}{\sqrt{2}}\eta+\frac{v_2}{\sqrt{2}}\xi\right)V_R^\dagger \tag{A6}$$

and either solve for ξ (rotation of type a)

$$\xi=\frac{\sqrt{2}}{v_2}V_L^\dagger M_l^{\rm diag}V_R-\frac{v_1}{v_2}\eta \tag{A7}$$

or for η (rotation of type b)

$$\eta=\frac{\sqrt{2}}{v_1}V_L^\dagger M_l^{\rm diag}V_R-\frac{v_2}{v_1}\xi. \tag{A8}$$

In terms of η the leptonic Lagrangian reads (type a)

$$\begin{aligned}\mathcal{L}^a=&-\frac{m_i}{v\sin\beta}\bar{l}_i l_i(\cos\alpha\ \ h^0+\sin\alpha\ \ H^0)\\ &-i\frac{m_i\cot\beta}{v}\bar{l}_i\gamma_5 l_i A^0-\frac{m_i\cot\beta}{\sqrt{2}v}\bar{n}_i(1+\gamma_5)l_i H^+\\ &+\frac{1}{\sqrt{2}\sin\beta}\bar{l}_i\eta_{ij}l_j[\cos(\alpha-\beta)h^0+\sin(\alpha-\beta)H^0]\\ &+\frac{i}{\sqrt{2}\sin\beta}\bar{l}_i\eta_{ij}\gamma_5 l_j A^0+\frac{1}{2\sin\beta}\bar{n}_i\eta_{ij}(1+\gamma_5)l_j H^+\\ &+\text{H.c.}\end{aligned} \tag{A9}$$

while in terms of ξ the leptonic Lagrangian reads (type b)

$$\begin{aligned}\mathcal{L}^b=&-\frac{m_i}{v\cos\beta}\bar{l}_i l_i(\sin\alpha\ \ h^0-\cos\alpha\ \ H^0)\\ &+i\frac{m_i\tan\beta}{v}\bar{l}_i\gamma_5 l_i A^0+\frac{m_i\tan\beta}{\sqrt{2}v}\bar{n}_i(1+\gamma_5)l_i H^+\\ &-\frac{1}{\sqrt{2}\cos\beta}\bar{l}_i\xi_{ij}l_j[\cos(\alpha-\beta)h^0+\sin(\alpha-\beta)H^0]\\ &-\frac{i}{\sqrt{2}\cos\beta}\bar{l}_i\xi_{ij}\gamma_5 l_j A^0-\frac{1}{2\cos\beta}\bar{n}_i\xi_{ij}(1+\gamma_5)_j H^+\\ &+\text{H.c.}\end{aligned} \tag{A10}$$

where n is the neutrino field, $v=(\sqrt{2}\ G_F)^{-1/2}=246$ GeV is the SM vacuum expectation value, related to v_1 and v_2 by

$$v=\sqrt{v_1^2+v_2^2}. \tag{A11}$$

Note that the Lagrangian (A9) corresponds in the lepton flavor conserving part to 2HDM-I, while the Lagrangian (A10) to 2HDM-II.

The couplings for lepton flavor conserving and violating Yukawa interactions h_{ij} can be read directly from the Lagrangian (A9) and (A10). As an example the lepton flavor conserving charged Higgs coupling squared from Eq. (A10) (which is the same as in 2HDM-II) is

$$h_{\mu\nu}^2=\frac{m_\mu^2\tan^2\beta}{2v^2}=\frac{G_F m_\mu^2\tan^2\beta}{\sqrt{2}} \tag{A12}$$

in agreement with the erratum in [1] (see the discussion there for a comment on other results in the literature).

We give in the following the complete expressions for the widths used in the analysis. For the tree-level widths we do not give here loop contributions and threshold effects, but those effects are taken into account in the numerical calculation of the branching ratios. The decays of a *CP*-even or -odd neutral Higgs boson to a pair of fermions are

TABLE XI. The mixing angles for the neutral Higgs bosons decays to fermions; u refers to up-type quarks, d to down-type quarks and leptons.

	MSSM	2HDM-III type a	2HDM-III type b
$\theta(h^0\to u\bar{u})$	$\cos\alpha/\sin\beta$	$\cos\alpha/\sin\beta$	$\sin\alpha/\cos\beta$
$\theta(h^0\to d\bar{d})$	$\sin\alpha/\cos\beta$	$\cos\alpha/\sin\beta$	$\sin\alpha/\cos\beta$
$\theta(h^0\to\tau\mu)$	0	$\cos(\alpha-\beta)/(\sqrt{2}\sin\beta)$	$\cos(\alpha-\beta)/(\sqrt{2}\cos\beta)$
$\theta(H^0\to u\bar{u})$	$\sin\alpha/\sin\beta$	$\sin\alpha/\sin\beta$	$\cos\alpha/\cos\beta$
$\theta(H^0\to d\bar{d})$	$\cos\alpha/\cos\beta$	$\sin\alpha/\sin\beta$	$\cos\alpha/\cos\beta$
$\theta(H^0\to\tau\mu)$	0	$\sin(\alpha-\beta)/(\sqrt{2}\sin\beta)$	$\sin(\alpha-\beta)/(\sqrt{2}\cos\beta)$
$\theta(A^0\to u\bar{u})$	$\cot\beta$	$\cot\beta$	$\tan\beta$
$\theta(A^0\to d\bar{d})$	$\tan\beta$	$\cot\beta$	$\tan\beta$
$\theta(A^0\to\tau\mu)$	0	$1/(\sqrt{2}\sin\beta)$	$1/(\sqrt{2}\cos\beta)$

$$\Gamma(H^0\to l_i^+ l_j^-)=m_H\frac{N_c\lambda_{ij}^2}{8\pi}\frac{m_i m_j}{v^2}\;\theta^2(\alpha,\beta)\times\left(1-\frac{(m_i+m_j)^2}{m_H^2}\right)^{3/2}\times\left(1-\frac{(m_i-m_j)^2}{m_H^2}\right)^{1/2},\qquad\text{(A13)}$$

$$\Gamma(A^0\to l_i^+ l_j^-)=m_A\frac{N_c\lambda_{ij}^2}{8\pi}\frac{m_i m_j}{v^2}\;\theta^2(\alpha,\beta)\times\left(1-\frac{(m_i+m_j)^2}{m_A^2}\right)^{1/2}\times\left(1-\frac{(m_i-m_j)^2}{m_A^2}\right)^{3/2},\qquad\text{(A14)}$$

where $N_c=3$ for quarks and $N_c=1$ for leptons. For a flavor conserving decay $\lambda_{ii}=1$ and $m_i=m_j$. $\theta(\alpha,\beta)$ is a function of the mixing parameters, given in Table XI. The Higgs couplings to gauge bosons follow from gauge invariance and are therefore model independent. There are no tree-level couplings of vector boson pairs to the charged Higgs boson $H^\pm$ and to the *CP*-odd neutral Higgs boson A. For the neutral *CP*-even sector:

$$\Gamma(h^0\to W^+W^-)=\frac{\sin^2(\beta-\alpha)}{16\pi v^2 m_h}(m_h^4-4m_h^2m_W^2+12m_W^4)\times\left(1-4\frac{m_W^2}{m_h^2}\right)^{1/2},\qquad\text{(A15)}$$

$$\Gamma(h^0\to ZZ)=\frac{\sin^2(\beta-\alpha)}{32\pi v^2 m_h}(m_h^4-4m_h^2m_Z^2+12m_Z^4)\times\left(1-4\frac{m_Z^2}{m_h^2}\right)^{1/2},\qquad\text{(A16)}$$

and the corresponding expressions for H^0 can be obtained replacing $\sin^2(\beta-\alpha)$ with $\cos^2(\beta-\alpha)$. The loop-induced decays to gg and $\gamma\gamma$ can be obtained from Chap. 2 and Appendix C of the first reference in [1] for the MSSM. For a generic neutral Higgs boson ϕ they are given by

$$\Gamma(\phi^0\to gg)=\frac{\alpha_s^2}{128\pi^3 v^2}m_\phi^3\left|\sum_i J_i^\phi\right|^2,\qquad\text{(A17)}$$

$$\Gamma(\phi^0\to\gamma\gamma)=\frac{\alpha_{em}^2}{256\pi^3 v^2}m_\phi^3\left|\sum_i I_i^\phi\right|^2,\qquad\text{(A18)}$$

TABLE XII. The coefficients C_i^ϕ; u refers to up-type quarks, d to down-type quarks and leptons.

	2HDM-III type a	2HDM-III type b
C_u^h	$\cos\alpha/\sin\beta$	$-\sin\alpha/\cos\beta$
C_d^h	$\cos\alpha/\sin\beta$	$-\sin\alpha/\cos\beta$
C_W^h	$\sin(\beta-\alpha)$	$\sin(\beta-\alpha)$
$C_{H^\pm}^h$	$g(h^0H^+H^-)$	$g(h^0H^+H^-)$
C_u^H	$\sin\alpha/\sin\beta$	$\cos\alpha/\cos\beta$
C_d^H	$\sin\alpha/\sin\beta$	$\cos\alpha/\cos\beta$
C_W^H	$\cos(\beta-\alpha)$	$\cos(\beta-\alpha)$
$C_{H^\pm}^H$	$g(H^0H^+H^-)$	$g(H^0H^+H^-)$
C_u^A	$-\cot\beta$	$\tan\beta$
C_d^A	$\cot\beta$	$-\tan\beta$
C_W^A	0	0
$C_{H^\pm}^A$	0	0

where the sum over the index i is limited to quarks for gg

$$J_q^h = C_q^\phi F_{1/2}(\tau_q) \tag{A19}$$

while it runs over fermions, W, $H^\pm$ for $\gamma\gamma$:

$$I_f^\phi = N_c e^2 C_f^\phi F_{1/2}(\tau_f) \tag{A20}$$

$$I_W^\phi = C_W^\phi F_1(\tau_W) \tag{A21}$$

$$I_{H^\pm}^\phi = C_{H^\pm}^\phi F_0(\tau_{H^\pm}) \frac{m_W^2}{m_{H^\pm}^2} \tag{A22}$$

where $\tau_i = 4m_i^2/m_\phi^2$, $N_c = 3$ for quarks, $N_c = 1$ for leptons, e is the electric charge in units of the charge of the electron, the functions F are given by

$$F_0 = \tau[1 - \tau g(\tau)] \tag{A23}$$

$$F_{1/2} = -2\tau[\delta + (1 - \delta\tau) g(\tau)] \tag{A24}$$

$$F_1 = 2 + 3\tau + 3\tau(2 - \tau) g(\tau) \tag{A25}$$

where $\delta = 1$ for h^0, H^0, and $\delta = 0$ for A. The function $g(x)$ is

$$g(x) = \begin{cases} a \sin^2(\sqrt{1/x}), & x \geq 1, \\ -\frac{1}{4}\left[\log \frac{1+\sqrt{1-x}}{1-\sqrt{1-x}} - i\pi\right], & x < 1. \end{cases} \tag{A26}$$

The coefficients C_i^ϕ are given in Table XII and the couplings $g(h^0 H^+ H^-)$, $g(H^0 H^+ H^-)$ of Table XII can be found in Appendix A of the last paper in [27].

[1] J.F. Gunion, H.E. Haber, G.L. Kane, and S. Dawson, *The Higgs Hunter's Guide* (Addison-Wesley, Reading, MA, 1990), Erratum: hep-ph/9302272; H.E. Haber and G.L. Kane, Phys. Rep. **117**, 75 (1985).

[2] T.P. Cheng and M. Sher, Phys. Rev. D **35**, 3484 (1987); A. Antaramian, L.J. Hall, and A. Rasin, Phys. Rev. Lett. **69**, 1871 (1992); L.J. Hall and S. Weinberg, Phys. Rev. D **48**, 979 (1993); M.J. Savage, Phys. Lett. B **266**, 135 (1991); M.E. Luke and M.J. Savage, *ibid.* **307**, 387 (1993).

[3] H.P. Nilles, Phys. Rep. **110**, 1 (1984).

[4] G.F. Giudice and R. Rattazzi, Phys. Rep. **322**, 419 (1999).

[5] R. Barbieri, G.R. Dvali, and L.J. Hall, Phys. Lett. B **377**, 76 (1996).

[6] L.J. Hall, V.A. Kostelecky, and S. Raby, Nucl. Phys. **B267**, 415 (1986).

[7] F. Borzumati and A. Masiero, Phys. Rev. Lett. **57**, 961 (1986).

[8] J. Ellis, M.E. Gomez, G.K. Leontaris, S. Sola, and D.V. Nanopoulos, Eur. Phys. J. C **14**, 319 (2000).

[9] J.L. Feng, Y. Nir, and Y. Shadmi, Phys. Rev. D **61**, 113005 (2000).

[10] J. Hisano, T. Moroi, K. Tobe, and M. Yamagushi, Phys. Rev. D **53**, 2442 (1996); Phys. Lett. B **391**, 341 (1997); J. Hisano, D. Nomura, and T. Yanagida, *ibid.* **437**, 351 (1998); J. Hisano and D. Nomura, Phys. Rev. D **59**, 116005 (1999); J. Hisano, M.M. Nojiri, Y. Shimizu, and M. Tanaka, *ibid.* **60**, 055008 (1999); J. Hisano, D. Nomura, Y. Okada, Y. Shimizu, and M. Tanaka, *ibid.* **58**, 116010 (1998); J. Hisano, hep-ph/9806222; hep-ph/9906312; J. Hisano and K. Kurosawa, hep-ph/0004061.

[11] M. Chaichian and K. Huitu, Phys. Lett. B **384**, 157 (1996); K. Huitu, J. Maalampi, M. Raidal, and A. Santamaria, *ibid.* **430**, 355 (1998).

[12] S.L. Glashow and S. Weinberg, Phys. Rev. D **15**, 1958 (1977).

[13] D. Bowser-Chao, K. Cheung, and W.-Y. Keung, Phys. Rev. D **59**, 115006 (1999).

[14] G. Buchalla, A. Buras, and M. Lautenbacher, Rev. Mod. Phys. **68**, 1125 (1996); A.J. Buras, M. Misiak, M. Munz, and S. Pokorski, Nucl. Phys. **B424**, 374 (1994).

[15] K. Chetyrkin, M. Misiak, and M. Munz, Phys. Lett. B **400**, 206 (1997); **425**, 414(E) (1998); M. Ciuchini, G. Degrassi, P. Gambino, and G.F. Giudice, Nucl. Phys. **B527**, 21 (1998); A. Kagan and M. Neubert, Eur. Phys. J. C **7**, 5 (1999).

[16] CLEO Collaboration, M.S. Alam, Phys. Rev. Lett. **74**, 2885 (1995); R. Briere, in Proceedings of ICHEP98, Vancouver, Canada, 1998, CLEO-CONF-98-17; and in (unpublished).

[17] ALEPH Collaboration, R. Barate, Phys. Lett. B **429**, 169 (1998).

[18] J.L. Hewett, Phys. Rev. Lett. **70**, 1045 (1993); V.D. Barger, M.S. Berger, and R.J. Phillips, *ibid.* **70**, 1368 (1993); F.M. Borzumati and C. Greub, Phys. Rev. D **58**, 074004 (1998); J.A. Coarasa, J. Guasch, J. Sola, and W. Hollik, Phys. Lett. B **442**, 326 (1998); F.M. Borzumati and C. Greub, Phys. Rev. D **59**, 057501 (1999); G. Degrassi, P. Gambino, and G.F. Giudice, J. High Energy Phys. **12**, 009 (2000); P. Gambino and M. Misiak, Nucl. Phys. **B611**, 338 (2001).

[19] D. Atwood, L. Reina, and A. Soni, Phys. Rev. D **55**, 3156 (1997).

[20] J.L. Diaz Cruz, J.J. Godina Nava, and G. Lopez Castro, Phys. Rev. D **51**, 5263 (1995).

[21] M. Sher and Y. Yuan, Phys. Rev. D **44**, 1461 (1991).

[22] S. Nie and M. Sher, Phys. Rev. D **58**, 097701 (1998).

[23] Muon g-2 Collaboration, H.N. Brown *et al.*, Phys. Rev. Lett. **86**, 2227 (2001); Muon g-2 Collaboration, G.W. Bennett *et al.*, *ibid.* **89**, 101804 (2002); **89**, 129903 (2002).

[24] M. Knecht and A. Nyffeler, Phys. Rev. D **65**, 073034 (2002); M. Knecht, A. Nyffeler, M. Perrottet, and E. De Rafael, Phys. Rev. Lett. **88**, 071802 (2002); I. Blokland, A. Czarnecki, and K. Melnikov, *ibid.* **88**, 071803 (2002); J. Bijnens, E. Pallante, and J. Prades, Nucl. Phys. **B626**, 410 (2002).

[25] M. Ramsey-Musolf and M.B. Wise, Phys. Rev. Lett. **89**, 041601 (2002).

[26] J.P. Leveille, Nucl. Phys. **B137**, 63 (1978).

[27] H.E. Haber and R. Hempfling, Phys. Rev. Lett. **66**, 1815 (1991); J.R. Ellis, G. Ridolfi, and F. Zwirner, Phys. Lett. B **257**, 83 (1991); Y. Okada, M. Yamaguchi, and T. Yanagida,

Prog. Theor. Phys. **85**, 1 (1991); H.E. Haber, hep-ph/9707213.
[28] J.A. Aguilar-Saavedra and G.C. Branco, Phys. Lett. B **495**, 347 (2000).
[29] S. Bejar, J. Guasch, and J. Sola, in Proceedings of the 5th International Symposium on Radiative Corrections (RADCOR 2000), edited by Howard E. Haber, hep-ph/0101294.
[30] T. Han, J. Jiang, and M. Sher, Phys. Lett. B **516**, 337 (2001).
[31] SuperKamiokande Collaboration, Y. Fukuda *et al.*, Phys. Rev. Lett. **82**, 2644 (1999); **85**, 3999 (2000); **86**, 5656 (2001).
[32] L. Serin and R. Stroynowski, ATLAS Internal Note, ATL-PHYS-97-114, 1997.
[33] I. Hinchliffe and F.E. Paige, Phys. Rev. D **63**, 115006 (2001).
[34] J.L. Diaz-Cruz and J.J. Toscano, Phys. Rev. D **62**, 116005 (2000).
[35] M. Sher, Phys. Lett. B **487**, 151 (2000).
[36] U. Cotti, L. Diaz-Cruz, C. Pagliarone, and E. Vataga, in Proceedings of the APS/DPF/DPB Summer Study on the Future of Particle Physics (Snowmass 2001), edited by R. Davidson and C. Quigg, hep-ph/0111236.
[37] A. Djouadi, J. Kalinowski, and M. Spira, Comput. Phys. Commun. **108**, 56 (1998).
[38] T. Sjöstrand, Comput. Phys. Commun. **82**, 74 (1994); T. Sjöstrand, P. Eden, C. Friberg, L. Lonnblad, G. Miu, S. Mrenna, and E. Norrbin, *ibid.* **135**, 238 (2001); T. Sjöstrand, L. Lonnblad, and S. Mrenna, hep-ph/0108264.
[39] H.L. Lai *et al.*, Phys. Rev. D **55**, 1280 (1997).
[40] E. Richter-Wąs, D. Froidevaux, and L. Poggioli, ATLAS Internal Note, ATL-PHYS-98-131, 1998.
[41] M. Spira, hep-ph/9510347.
[42] S. Balatenychev *et al*., ''Theoretical Developments,'' in [53], p. 4, and the references therein.
[43] S. Catani, D. de Florian, and M. Grazzini, J. High Energy Phys. **01**, 015 (2002).
[44] S. Frixione, P. Nason, and G. Ridolfi, Nucl. Phys. **B383**, 3 (1992); S. Frixione, *ibid.* **B410**, 280 (1993); U. Baur, T. Han, and J. Ohnemus, Phys. Rev. D **48**, 5140 (1993); **51**, 3381 (1995); **53**, 1098 (1996); **57**, 2823 (1998).
[45] L.J. Dixon, Z. Kunszt, and A. Signer, Phys. Rev. D **60**, 114037 (1999).
[46] J. Campbell and R.K. Ellis, Phys. Rev. D **65**, 113007 (2002).
[47] S. Jadach, Z. Wąs, R. Decker, and J.H. Kühn, Comput. Phys. Commun. **76**, 361 (1993); M. Jezabek, Z. Wąs, S. Jadach, and J.H. Kühn, *ibid.* **70**, 69 (1992); S. Jadach, J.H. Kühn, and Z. Wąs, *ibid.* **64**, 275 (1990).
[48] T. Han and D. Marfatia, Phys. Rev. Lett. **86**, 1442 (2001).
[49] D. Rainwater, D. Zeppenfeld, and K. Hagiwara, Phys. Rev. D **59**, 014037 (1999); L. Di Lella, Proceedings of the Large Hadron Collider Workshop, Aachen, 1990, Vol. II, p. 183, edited by G. Jarlskog and D. Rein, CERN 90-10/ECFA 90-133.
[50] ATLAS Collaboration, ''ATLAS Detector and Physics Performance Technical Design Report,'' CERN/LHCC/99-15, 1999, p. 742; D. Cavalli *et al.*, ATLAS Internal Note ATL-PHYS-94-051; ''Study of the MSSM channel $A/H \rightarrow \tau\tau$ at the LHC,'' in [53], p. 67.
[51] R. Kinnunen and D. Denegri, CMS NOTE 1999/037, hep-ph/9907291; A. Nikitenko, S. Kunori, and R. Kinnunen, CMS Note 2001/040; D. Denegri *et al.*, CMS NOTE 2001/032, hep-ph/0112045.
[52] R.A. Diaz, R. Martinez, and J. Alexis Rodriguez, Phys. Rev. D **63**, 095007 (2001); **64**, 033004 (2001).
[53] D. Cavalli *et al.*, ''The Higgs working group: Summary report,'' hep-ph/0203056.